BRAIN
ORIGINAL ARTICLE

Stimulation of the cuneiform nucleus enables training and boosts recovery after spinal cord injury

Anna-Sophie Hofer,[1,2,3] Myriam I. Scheuber,[1,2,3] Andrea M. Sartori,[1,2,3,†] Nicolas Good,[1,2,3] Stephanie A. Stalder,[1,3] Nicole Hammer,[2,3] Kai Fricke,[1,3] Sina M. Schalbetter,[1,2,3] Anne K. Engmann,[1,3,‡] Rebecca Z. Weber,[1,2,3] Ruslan Rust,[1,2,3] Marc P. Schneider,[1,3] Natalie Russi,[1,3] Giacomin Favre[4] and Martin E. Schwab[1,2,3]

Severe spinal cord injuries result in permanent paraparesis in spite of the frequent sparing of small portions of white matter. Spared fibre tracts are often incapable of maintaining and modulating the activity of lower spinal motor centres. Effects of rehabilitative training thus remain limited.

Here, we activated spared descending brainstem fibres by electrical deep brain stimulation of the cuneiform nucleus of the mesencephalic locomotor region, the main control centre for locomotion in the brainstem, in adult female Lewis rats.

We show that deep brain stimulation of the cuneiform nucleus enhances the weak remaining motor drive in highly paraparetic rats with severe, incomplete spinal cord injuries and enables high-intensity locomotor training. Stimulation of the cuneiform nucleus during rehabilitative aquatraining after subchronic ($n = 8$ stimulated versus $n = 7$ unstimulated versus $n = 7$ untrained rats) and chronic ($n = 14$ stimulated versus $n = 9$ unstimulated versus $n = 9$ untrained rats) spinal cord injury re-established substantial locomotion and improved long-term recovery of motor function. We additionally identified a safety window of stimulation parameters ensuring context-specific locomotor control in intact rats ($n = 18$) and illustrate the importance of timing of treatment initiation after spinal cord injury ($n = 14$).

This study highlights stimulation of the cuneiform nucleus as a highly promising therapeutic strategy to enhance motor recovery after subchronic and chronic incomplete spinal cord injury with direct clinical applicability.

1 Brain Research Institute, University of Zurich, 8057 Zurich, Switzerland
2 Institute for Regenerative Medicine, University of Zurich, 8952 Schlieren, Switzerland
3 Department of Health Sciences and Technology, ETH Zurich, 8092 Zurich, Switzerland
4 Department of Economics, University of Zurich, 8032 Zurich, Switzerland

† Present address: Department of Medicine, Harvard Medical School, Beth Israel Deaconess Medical Center, Boston, MA, USA
‡ Present address: Department of Stem Cell and Regenerative Biology, Harvard University, Cambridge, MA, USA

Correspondence to: Anna-Sophie Hofer
Institute for Regenerative Medicine, University of Zurich
Wagistrasse 12, 8952 Schlieren, Switzerland
E-mail: hofer@irem.uzh.ch

Received January 01, 2022. Revised April 07, 2022. Accepted May 04, 2022. Advance access publication May 18, 2022

Keywords: spinal cord injury; rehabilitative training; deep brain stimulation; mesencephalic locomotor region; cuneiform nucleus

Abbreviations: BBB score = Basso, Beattie, Bresnahan locomotor score; CNF = cuneiform nucleus; DBS = deep brain stimulation; DBS/TR = DBS+ training group; dpi = day(s) post-injury; MLR = mesencephalic locomotor region; NRG = gigantocellular reticular nucleus; PPN = pedunculopontine nucleus; SCI = spinal cord injury; TH = motor threshold; TR = training only group; vGAT = vesicular GABA transporter

Introduction

Neurorehabilitation is the only treatment available for patients with spinal cord injury (SCI). However, effects on motor recovery are limited even with incomplete injuries.[1] Locomotion is a complex motor behaviour involving timed and harmonized recruitment of a multitude of muscles,[2] generated by brain-controlled motor circuits in the spinal cord.[2,3] During initiation of locomotion, these central pattern generators (CPGs) become active,[4,5] and their activity is regulated by descending input from brainstem motor centres.[4,6] An evolutionarily conserved, key command centre is the mesencephalic locomotor region (MLR), comprising the pedunculopontine (PPN) and cuneiform (CNF) nuclei. It initiates stepping and regulates locomotor rhythm and pattern.[6,7] Electrical stimulation of the MLR in vertebrates can manipulate locomotor speed and pattern in an intensity-dependent manner.[8–10] It projects to the medial medullary reticular formation[11,12] and indirectly activates the spinal CPGs via the reticulospinal tract system.[13,14] In most patients with SCI, the communication between brainstem and sublesional spinal cord is incompletely disrupted[15–17] while CPGs remain intact due to their lumbar location. However, spared supraspinal input is often insufficient for proper modulation of CPGs, which fail to translate multisensory feedback information into a motor pattern.[18] Thus, locomotor recovery remains limited. Electrical stimulation of spinal[19–21] and brainstem locomotor centres[22] are novel strategies to elevate the excitability of spinal neuronal circuits. Transcutaneous,[23–26] epidural[27–31] or intraspinal[32] stimulation have been shown to facilitate motor function after SCI in animal models and human case studies. Acute deep brain stimulation (DBS) of the MLR transiently improved hindlimb stepping in a first study in rats with incomplete SCI.[22] DBS is considered minimally invasive and safe,[33] and stimulating the PPN[34,35] and CNF[36] can reduce locomotor symptoms associated with Parkinson's disease. Even though the relative contribution of PPN and CNF to observed locomotor effects is still a matter of debate,[6,37] current literature suggests the CNF as promising target for therapeutic DBS to improve impaired locomotion after neurotrauma.[38–41] We hypothesize that DBS of the CNF enhances the efficacy of activity-based rehabilitation to re-enable functional locomotor patterns, improving long-term outcome.[42] The potential of CNF-DBS to improve gait in non-ambulatory, chronic SCI patients is currently being investigated in a first in-man proof-of-concept trial (https://clinicaltrials.gov, DBS-SCI, Identifier: NCT03053791).[43] In the present study, we first identified the safety window of stimulation parameters for CNF-DBS preserving controlled locomotor behaviour adapted to context in intact rats. We then show that the therapeutic effects of CNF-DBS on motor recovery appear progressively in the subchronic and chronic post-injury phases. Ultimately, we activated residual descending reticulospinal connections during rehabilitative aquatraining with CNF-DBS in rats with severe, incomplete SCI and show that CNF-DBS enables high-intensity training, enhances stepping and promotes long-term gait recovery.

Materials and methods

Experimental design

Animals

Adult female Lewis rats (220–250 g; Janvier; $n = 127$) were group-housed at a 12:12-h light:dark cycle with food and water *ad libitum*. Seven days of acclimatization were granted before any experiment. Behavioural testing took place during light phase, rehabilitative training during animals' active phase. Experimental procedures and animal care were conducted in accordance with ethical guidelines, conform to ARRIVE[44] guidelines and were approved by the Veterinary Office of the Canton of Zurich, Switzerland.

Experiments

To identify stimulation parameters ensuring context-specific locomotor behaviour, different types of movement control with and without CNF-DBS were investigated in two cohorts of intact animals (Fig. 1): (i) control over locomotor pattern, $n = 6$ (Fig. 1A–F); and (ii) place preference, obstacle avoidance capability, speed control, $n = 12$ (Fig. 1G–I). For anatomical correlation, retrograde Fast Blue tracing of the CNF was performed in $n = 5$ intact animals (Fig. 1J and K).

Time-dependent therapeutic efficacy of acute CNF-DBS was evaluated in $n = 14$ animals (Fig. 2 and Supplementary Figs 2 and 3) by comparing walking performance without stimulation to walking performance under stimulation weekly after SCI for 5 weeks (Fig. 2A). Injury-induced plasticity of CNF fibres projecting to the gigantocellular reticular nucleus (NRG) was assessed in an anterograde tracing timeline study with $n = 29$ animals randomly assigned to either of four groups (Fig. 3): intact group ($n = 6$); group perfused on day post-injury (dpi) 7 ($n = 8$); dpi14 ($n = 8$); dpi35 ($n = 7$). One animal was excluded due to off-target tracer injection.

The therapeutic potential of repeated CNF-DBS-enabled high-intensity training after severe SCI was evaluated in $n = 61$ animals, which were stratified randomized into a subchronic ($n = 28$, Figs 4, 6 and Supplementary Figs 4–6) and a chronic ($n = 33$, Figs 5, 6 and Supplementary Figs 4–6) cohort. Animals of the subchronic/chronic cohort were stratified [Basso, Beattie, Bresnahan (BBB) locomotor score, weight] randomized and allocated to three different rehabilitation paradigms: DBS/TR ($n = 12/n = 14$), undergoing daily high-intensity aquatraining enabled by CNF-DBS for 6 weeks; TR ($n = 8/n = 10$), undergoing low-intensity aquatraining without DBS; and control (Control; $n = 8/n = 9$), receiving no training. Six subchronic and one chronic animal were excluded retrospectively due to complete lesions. Changes in BBB scores and kinematic parameters are primary readouts. Secondary readouts are the expression of vesicular GABA transporter (vGAT) and 5-hydroxytryptamine (5HT) in ventral horn and lamina X of lumbar levels L2 and L5 in representative animals of the subchronic cohort (DBS/TR: $n = 6$; TR: $n = 6$; Control: $n = 3$; Fig. 4L and M) and effects on bladder function (Fig. 6).

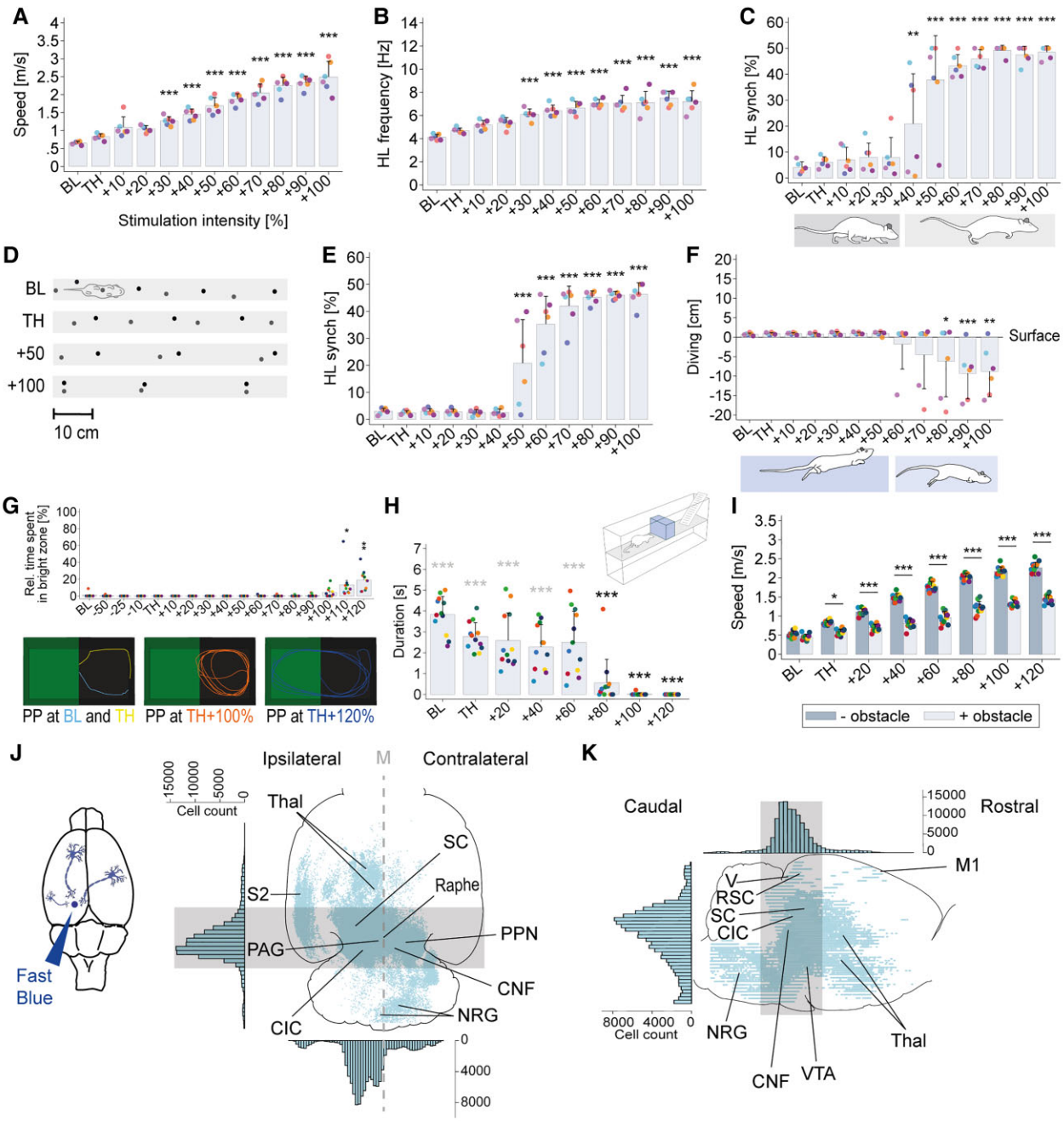

Figure 1 Safety window for CNF-DBS ensuring context-specific locomotor control in intact rats and CNF input structures. (**A**) Gradual increase in overall speed with CNF-DBS ($n = 6$). (**B**) Increase in hindlimb (HL) stepping frequency with CNF-DBS ($n = 6$). (**C**) Intensity-dependent temporal hindlimb step synchronization (synch; $n = 6$) during over-ground locomotion. (**D**) Representative footprint pattern illustrating intensity-dependent transition from walking to galloping. (**E**) Temporal hindlimb stroke synchronization with CNF-DBS during swimming ($n = 6$). (**F**) Over-ground gallop (diving) during swimming with high stimulation intensities ($n = 6$). (**G**) *Top row* (bar chart): relative (rel.) time spent in the bright zone during place preference (PP) testing with CNF-DBS ($n = 11$). High-intensity CNF-DBS (≥110%) interferes with animals' natural place preference for dark zone. *Bottom row*: representative movement trajectories at different stimulation intensities illustrating general preference for darkness. (**H**) Obstacle avoidance capability is impaired with high stimulation intensities ($n = 12$). Black asterisks: halting duration in front of obstacle versus baseline halting duration; grey asterisks: halting duration versus no delay (0 s). (**I**) Speed in presence versus absence of an obstacle ($n = 12$). The ability to adapt speed in presence of an obstacle persists at all stimulation intensities. (**J** and **K**) Reconstruction of Fast Blue-labelled CNF-input structures in (**J**) horizontal and (**K**) sagittal projection ($n = 5$). Histograms show total cell count and distribution. Grey area indicates region of highest cell count. CIC/SC = inferior/superior colliculus; M = midline; PAG = periaqueductal grey; Raphe = nucleus raphe; RSC = retrosplenial cortex; S2 = secondary somatosensory cortex; Thal = thalamus; V = visual cortex; VTA = ventral tegmental area. (**A–F**) One-way repeated-measures (intensity) ANOVA ($P < 0.001$). (**G–I**) Two-way repeated-measures (run and intensity; obstacle Y/N and intensity) ANOVA ($P < 0.001$). ANOVAs followed by Bonferroni *post hoc* testing comparing each parameter at each stimulation intensity with baseline (except **I**). $^{*}P < 0.05$, $^{**}P < 0.01$, $^{***}P < 0.001$. Data are presented as mean + SD in (**A–F**) and (**H** and **I**); as mean + SEM in (**G**). Coloured dots in **A–C** and **E–I** represent individual animals; *x*-axis = stimulation intensity in per cent of individual motor threshold (TH). Mean threshold intensity: 30.61 ± 9.52 µA in **A–F**; 28.17 ± 10.98 µA in **G–I**. BL = baseline (no stimulation).

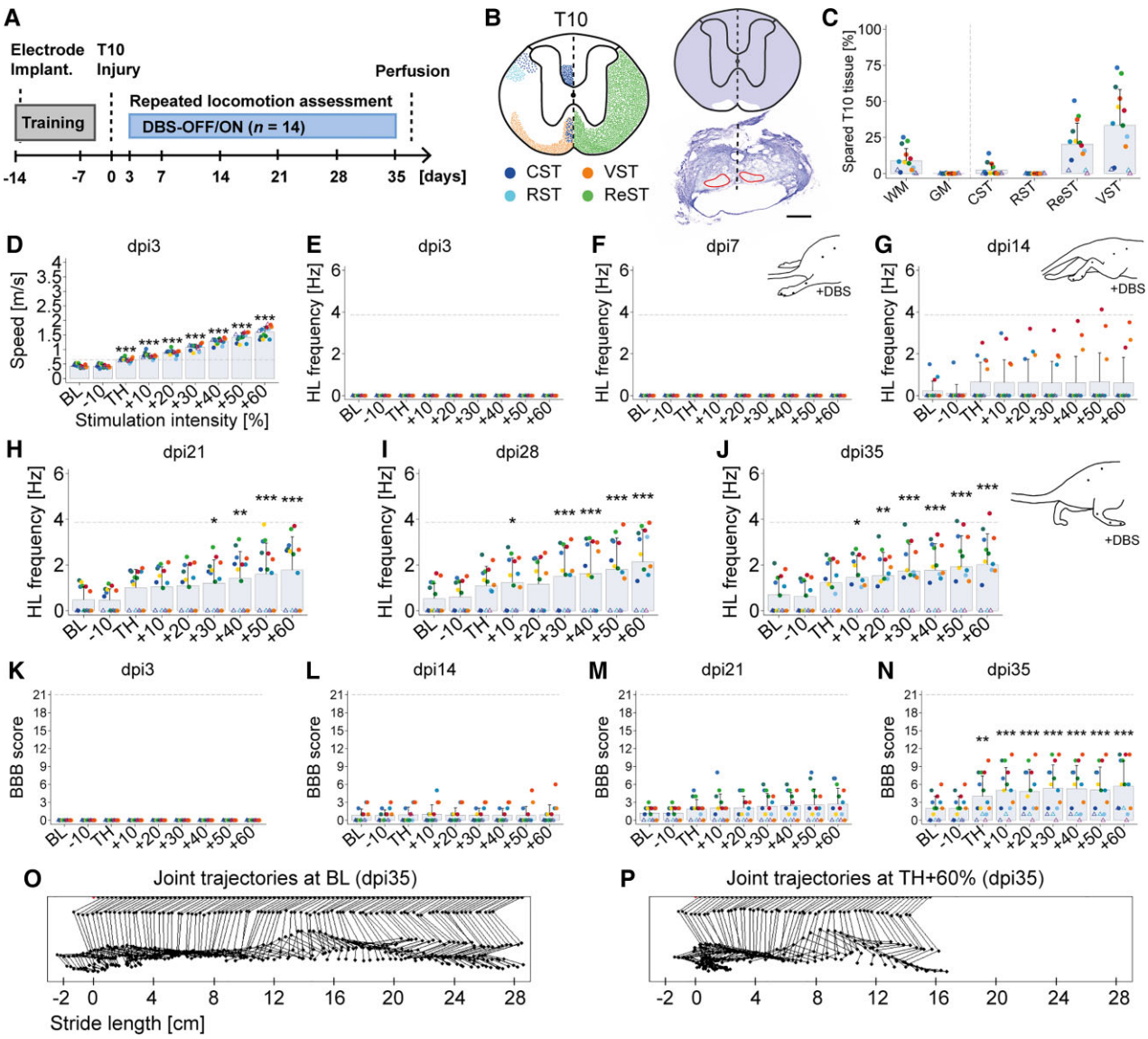

Figure 2 CNF-DBS acutely enhances hindlimb function only in subchronic and chronic SCI. (**A**) Timeline. (**B**) *Left*: Schematic illustration of intact main descending motor tracts at spinal level T10 (based on spinal cord atlas[45] and neuroanatomical studies[22]). CST (blue) = corticospinal tract; RST (light blue) = rubrospinal tract; VST (orange) = vestibulospinal tract; ReST (green) = reticulospinal tracts, including mesencephalic, medullary and pontine fibres. *Right*: Reconstructed spared (white) and destroyed (purple) tissue at lesion site (*top*) and respective Nissl-stained section (*bottom*). Black dashed lines = midline; red lines = spared tissue. Scale bar = 500 µm. (**C**) Quantification of spared spinal cord tissue and tracts. GM = grey matter; WM = white matter. (**D**) Overall speed increases with CNF-DBS 3 days post-injury (dpi). (**E–J**) Hindlimb (HL) stepping frequency 3–35 days post-injury with and without CNF-DBS. (**E** and **F**) No hindlimb stepping is elicited upon CNF-DBS on (**E**) dpi3 and (**F**) dpi7. (**G**) First animals exhibit hindlimb movements upon CNF-DBS on dpi14. (**H–J**) Re-establishment of functional hindlimb stepping on dpi21–35 with suprathreshold CNF-DBS in animals with bilateral ventromedial fibre sparing. (**K–N**) BBB scores during CNF-DBS on (**K**) dpi3; (**L**) dpi14; (**M**) dpi21; and (**N**) dpi35. (**O** and **P**) Representative joint trajectories showing step cycle (**O**) at baseline and (**P**) with TH +60% DBS on dpi35. (**C–N**) $n = 14$. (**D–N**) Two-way repeated-measures (time point and intensity) ANOVA ($P < 0.001$) followed by Bonferroni *post hoc* testing comparing parameters at each stimulation intensity with baseline of respective day. $^{*}P < 0.05$, $^{**}P < 0.01$, $^{***}P < 0.001$. Data are presented as mean + SD. (**C–N**) Rats represented by dots: 1% to 25% bilateral, ventromedial fibre sparing ($n = 11$); by triangle: unilateral fibre sparing (0.5% to 2%, $n = 2$) or complete lesion (0%, $n = 1$; Supplementary Fig. 2). (**D–N**) Grey dashed horizontal line represents intact mean baseline value. BL = baseline (no stimulation); TH = individual motor threshold (mean threshold intensity: 46.07 ± 30.77 µA). *X*-axis in **D–N** = stimulation intensity expressed as per cent of individual TH.

Surgery

Unilateral electrode implantation

For electrode implantation into the left CNF (Supplementary material and Supplementary Fig. 1), animals were anaesthetized with 5% isoflurane (Piramal Healthcare) followed by intramuscular injection of ketamine (70 mg/kg Ketalar, Pfizer), and head-fixed in a stereotaxic frame (David Kopf Instruments) with precise alignment of bregma and lambda in the mediolateral (ML) and dorsoventral (DV) plane. After skull exposure, three stainless-steel anchor and grounding screws were positioned across parietal and frontal bones, followed by craniotomy. Animals were positioned in a hammock on a warming pad ensuring full range of motion of tail, forelimbs and hindlimbs, followed by intraoperative stimulation (50 Hz, 0.5 ms pulse width). Initial stimulation was

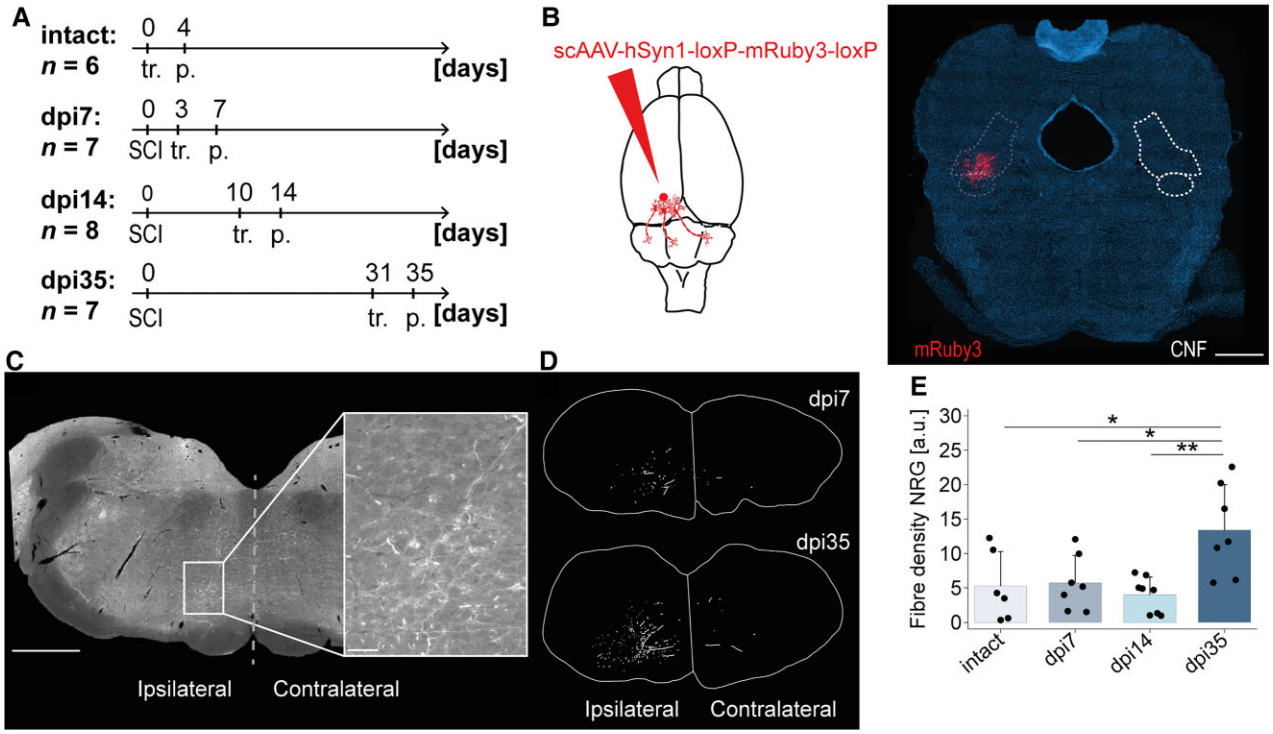

Figure 3 Delayed hindlimb response to CNF-DBS is paralleled by a lag in anatomical plasticity after T10 injury. (**A**) Experimental schedule to study CNF plasticity by comparing four groups: intact ($n = 6$), 7 days after injury ($n = 7$), 14 days after injury ($n = 8$), 35 days after injury ($n = 7$). dpi = day post-injury. tr. = tracing; p. = perfusion. (**B**) Schematic illustration and representative scAAV-DJ/2-hSyn1-chl-loxP-mRuby3-loxP-SV40p(A) injection site at AP −7.8 confined to the CNF (white dashed line). Scale bar = 1 mm. (**C**) Representative brainstem cross-section showing descending CNF fibres in the ipsi- and contralateral NRG. *Inset* shows high magnification of area rich in fibres. Dashed grey vertical line represents midline. Scale bars = 1 mm (overview); 100 µm (*inset*). (**D**) Representative reconstructions of CNF fibres in ipsilateral and contralateral NRG at dpi7 and dpi35. (**E**) Quantification of CNF fibre density in the ipsilateral NRG in intact ($n = 6$) and injured (dpi7: $n = 7$; dpi14: $n = 8$; dpi35: $n = 7$) animals, normalized to the number of infected cells in the CNF, shows a significant increase in fibre density 35 days after injury. a.u. = arbitrary unit. Dpi7, dpi14 and dpi35 indicate day of perfusion. One-way (group) ANOVA ($P < 0.01$) followed by Bonferroni *post hoc* testing. $^{*}P < 0.05$, $^{**}P < 0.01$, $^{***}P < 0.001$. Data are presented as mean + SD, dots represent single animals.

performed at Bregma anterior–posterior (AP) −7.8 mm, ML +2.0 mm and DV (dura) −4.7 mm (AP −7.8/ML + 2.0/DV −4.7/0°). Electrode positioning was adjusted in -0.1 mm steps until alternating, rhythmic bilateral stepping was elicited (28.84 ± 12.71 µA). Final implantation sites were AP −7.8/ML + 2.0/DV −5.1 to −5.5. The electrode was secured, wires were tightly connected to grounding screws and implants were fixed to skull and screws with light-hardened dental cement (Tetric Evoflow, Ivoclar Vivadent). The scalp was sutured and attached to the cement cap with Histoacryl (B. Braun). Correct positioning and functionality of electrodes was confirmed 7 days later in the open field (120 × 60 × 35 cm) by an intensity-dependent increase in speed and regularly reconfirmed. All animals were treated with antibiotics (Bactrim, 15 mg/kg bodyweight, Roche) and analgesics (Rimadyl, 2.5 mg/kg body weight, Pfizer) subcutaneously for 7 days.

Retrograde CNF tracing

Rats were anaesthetized with isoflurane and ketamine, head-fixed and positioned identical to electrode implantation. After craniotomy, intraoperative stimulation (50 Hz, 0.5 ms) was performed using a 33-gauge needle (NanoFil, World Precision Instruments) attached to a 10 µl syringe (Hamilton) driven by an electric microinjection pump (World Precision Instruments, UMC4). Needle positioning was adjusted in −0.1 mm steps starting at AP −7.8/ML +2.0/DV −4.7/0° in relation to Bregma until proper hindlimb stepping was initiated upon stimulation. Fast Blue (FB), 2 × 50 nl (EMS Chemie, 2% in DMSO; 100 nl/s), was injected 200 µm above the site showing the best hindlimb response. The needle was left in place for 5 min between injections and 15 min after the last injection to prevent tracer backflow, followed by skin suturing. Animals received Bactrim and Rimadyl daily and were perfused after 7 days.

Anterograde CNF tracing

Animals were anaesthetized with a triple-combinatorial preparation of medetomidine (Dormitor, 0.105 mg/kg body weight, Provet AG), midazolam (Dormicum®, 1.4 mg/kg body weight, Roche) and fentanyl (0.007 mg/kg body weight, Kantonsapotheke Zürich), head-fixed and placed on a warming pad. scAAV-DJ/2-hSyn1-chl-loxP-mRuby3-loxP-SV40p(A), 2 × 60 nl (Viral Vector Core Zurich, 7.2×10^{12} vg/ml; 6 nl/s), was injected into the left CNF at AP −7.8/ML +2.0/DV −5.3/0° using a NanoFil syringe connected to a 33-gauge needle with an attached microinjection pump. The needle was left in place for 2 min between injections and 3 min after the last injection to prevent tracer backflow. Skin was sutured and animals recovered on a heat blanket for 25 min before anaesthesia was antagonized by subcutaneous antidote

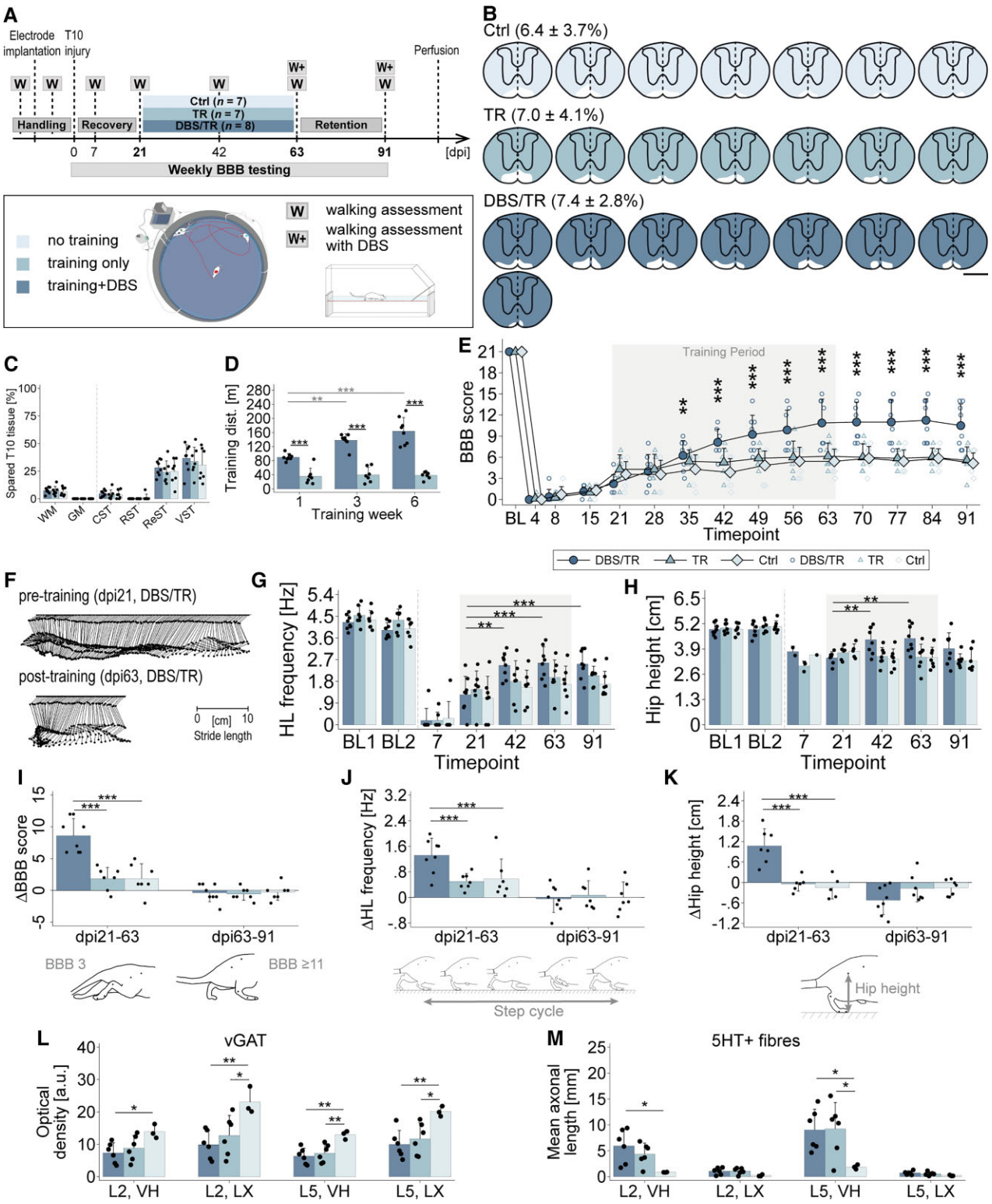

Figure 4 Long-term CNF-DBS initiated in the subchronic post-injury phase enables high-intensity training and improves hindlimb locomotion. (**A**) Study timeline and study groups: Control (Ctrl) = no training ($n = 7$); TR = training only ($n = 7$); DBS/TR = training + DBS ($n = 8$; mean stimulation intensity: 49.53 ± 11.51 μA). (**B**) Reconstructed, individual lesion sizes of each group. Fraction of spared tissue (white) shown as mean ± SD in %. Scale bar = 1 mm. (**C**) Comparable lesion sizes between groups. CST = corticospinal tract; GM = grey matter; ReST = reticulospinal tracts; RST = rubrospinal tract; VST = vestibulospinal tract; WM = white matter. One-way (group) ANOVA ($P > 0.05$) followed by Bonferroni *post hoc* test. (**D**) Training distances (dist.) on representative day of Weeks 1, 3, 6. 2(group) × 3(time point) mixed-factorial ANOVA ($P < 0.001$) followed by Bonferroni *post hoc* testing. Black asterisks: intergroup comparison of trained distance at each time point; grey asterisks: intragroup comparison of trained distance between time points. (**E**) Recovery of average BBB scores by group over time compared to pretreatment level (dpi21). BL = post-implantation baseline. X-axis: numbers indicate days post-injury (dpi);

(Continued)

application (Antisedan, 0.75 mg/kg body weight, Provet AG; Anexate, 1 mg/kg body weight, Roche). Animals received Bactrim and Rimadyl daily and were perfused after 4 days.

Spinal cord injury

Animals were anaesthetized with medetomidine, midazolam and fentanyl and positioned on a warming pad. A T8 laminectomy was performed, and the dura was carefully incised after application of additional 10 µl fentanyl intramuscularly and 1 ml glucose–Ringer solution (Fresenius Medical Care) subcutaneously. A severe, subtotal SCI at spinal level T10 was performed by repeated transections with iridectomy scissors, sparing only ventromedial fibre tracts bilaterally. Skin was sutured and animals recovered on a heat blanket for 45 min prior to antidote administration. In addition to standard postoperative care with Bactrim and Rimadyl for 14 days, animals received subcutaneous injections of glucose–Ringer solution if needed, and high-energy food was offered daily. Bladders were manually emptied twice a day throughout the entire study period. For spinal shock monitoring, manual hindlimb stretch reflex testing[47] was performed daily during the first 14 days. Stretch reflex was considered positive if hindlimb stretching elicited hindlimb muscle contractions.

Behaviour assessment and analysis

Deep brain stimulation

During behaviour assessments involving acute CNF-DBS (0.5 ms cathodal pulses; 50 Hz frequency; impulse generator and stimulus isolator by Word Precision Instruments) animals performed baseline runs without stimulation and runs at different stimulation intensities, expressed as per cent of motor threshold intensity. Each individual's motor threshold (TH) was determined directly before each testing in the respective assessment setup by slowly increasing stimulation intensity in 1–2 µA steps, starting either at 5 µA or 15 µA below last known TH. During testing, motor thresholds were verified regularly. An individual's motor threshold equals the lowest stimulation intensity reproducibly initiating stepping movements, walking (including stop and go), or acceleration during ongoing locomotion. Behaviours such as alertness, pausing and changes in breathing rate were considered as non-locomotor phenotypes and were observed at submotor threshold intensities.

Kinematic walking and swimming assessment

Walking assessment (with or without stimulation) was performed in a 150 × 40 × 13 cm transparent setup of duplex non-reflecting glass containing a 140 cm runway modified from a previous publication.[48] For swimming, the runway was removed and the tank filled with warm water (24–28°C) to a level of 24 cm. Before testing, bladder management was performed in injured animals, and iliac crest, hip, ankle and metatarsophalangeal (MTP) joints were marked. Hip and iliac crest were additionally tattooed during the handling period to ensure consistent and reliable markings over time. At least three high-quality videos showing animals from both sides and a ventral perspective were recorded with an immobile high-speed camera (200 frames/s, Basler A504kc Color Camera) per animal and condition. The video showing the best performance was selected, gait parameters were manually extracted using Fiji (ImageJ 1.50g, 64-bit version)[49] and normalized to a 60 cm distance on the runway. For definition of parameters we follow Bachmann *et al.*[22] (see Supplementary material for details).

Place preference testing

Rats were placed at the borderline between two compartments (60 × 60 × 35 cm each) of different visual properties (black/dark versus green/brightly illuminated) with free access to either zone. The relative time spent per zone without (3 min, 20 s) and with DBS (5 × 10 s stimuli/30 s break) at subthreshold to suprathreshold (TH −50% to TH +120%) intensities was recorded (one animal excluded due to implant failure). Videos were tracked automatically in EthoVision XT (Noldus).

Obstacle avoidance and speed control testing

An obstacle (8.5 × 13 × 15 cm) was placed in the last third of the runway of the kinematic assessment setup, allowing for vertical crossing only to reach the home cage containing treats. Each animal performed 5 consecutive runs without stimulation, at threshold and suprathreshold intensities up to TH +120%. Halting time prior to obstacle crossing was analysed for each run using frame-by-frame video analysis (Virtualdub). Naturally, rats stop and explore when encountering an obstacle; loss of obstacle avoidance capability was defined as a failure to halt prior to crossing. For assessment of speed control in presence versus absence of an obstacle, each animal performed runs with and without obstacle at baseline, at threshold and suprathreshold intensities up to TH +120%. Overall speed was analysed for one representative run for each condition per intensity and animal.

Basso, Beattie, Bresnahan locomotor scoring

BBB scoring[50] was performed by two researchers independently. Rats were placed in an open field individually and hindlimb motor activity was observed and rated for 4 min.

Rehabilitative training

DBS/TR and TR animals underwent daily aquatraining 5 days a week for 6 weeks (Figs 4A and 5A) in a circular, modified open field setup (160 cm diameter, 30 cm high; Fig. 4A) filled with shallow

Figure 4 Continued
3(group) × 11(time) mixed-factorial ANOVA ($P < 0.001$) followed by Bonferroni *post hoc* testing comparing performance at each time point after treatment start with pretreatment performance by group. (**F**) Representative joint trajectories of DBS/TR animal showing step cycle before and after training phase. (**G** and **H**) Improvement of (**G**) hindlimb (HL) stepping frequency and (**H**) hip height compared to pretreatment level (dpi21) during and beyond training phase. BL1/2 = baseline before/after electrode implantation; 3(group) × 4(time) mixed-factorial ANOVA ($P < 0.001$) followed by Bonferroni *post hoc* testing comparing performance at each time point after treatment start with pretreatment performance by group. (**I–K**) Intergroup comparison of changes in (**I**) BBB score, (**J**) stepping frequency and (**K**) hip height per period. dpi21–63 = training period. dpi63–91 = retention period; 3(group) × 3(period) mixed-factorial ANOVA ($P < 0.001$) followed by Bonferroni *post hoc* testing comparing change in parameter between groups by period. (**L**) Optical density of vesicular GABA transporter (vGAT), and (**M**) mean axonal length of serotonin (5HT)-positive fibres measured in ventral horns (VH) and lamina X (LX) of lumbar levels L2 and L5. DBS/TR: $n = 6$; TR: $n = 6$; Control: $n = 3$. (**L** and **M**) One-way (group) ANOVA followed by Bonferroni *post hoc* testing. *$P < 0.05$, **$P < 0.01$, ***$P < 0.001$. Data are presented as mean + SD. Scatter represents single animals. (**E**, **G** and **H**) Grey area marks training period. (**H** and **K**) Number of observations <n before dpi42 as hip height is unmeasurable until reappearance of ≥1 step cycle.

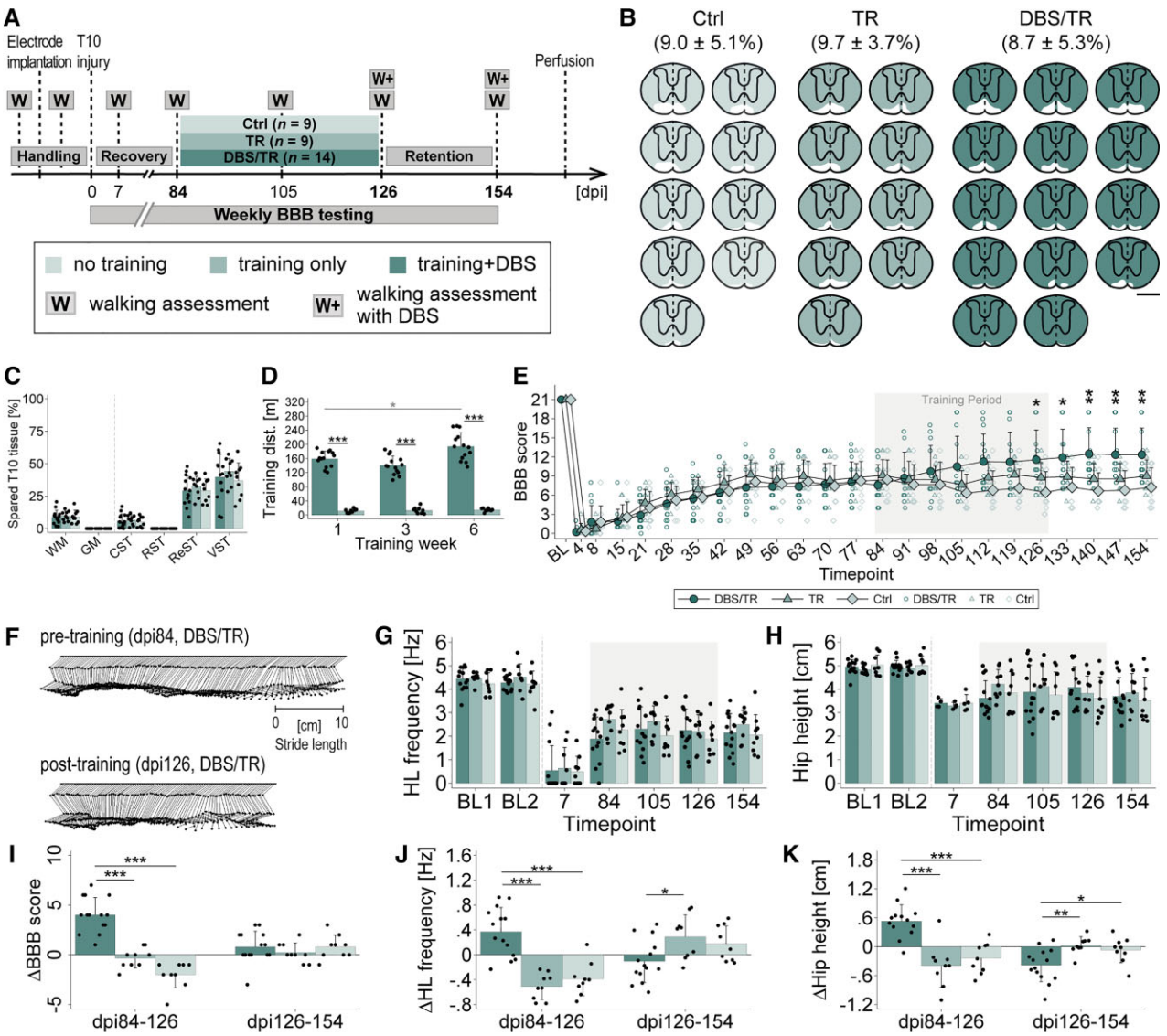

Figure 5 CNF-DBS enables rehabilitative training in late chronic stages after SCI and improves over-ground locomotion. (**A**) Study timeline and study groups: Control (Ctrl) = no training ($n = 9$); TR = training only ($n = 9$); DBS/TR = training + DBS ($n = 14$; mean stimulation intensity: 59.59 ± 10.81 μA). (**B**) Reconstructed, individual lesion sizes per group. Fraction of spared tissue (white) is shown as mean ± SD in %. Scale bar = 1 mm. (**C**) Comparable lesion sizes between groups. CST = corticospinal tract; GM = grey matter; ReST = reticulospinal tracts; RST = rubrospinal tract; VST = vestibulospinal tract; WM = white matter. One-way (group) ANOVA ($P > 0.05$) followed by Bonferroni *post hoc* test. (**D**) Training distance (dist.) covered by DBS/TR and TR animals on representative day of Weeks 1, 3, 6. 2(group) × 3(time point) mixed-factorial ANOVA ($P < 0.001$) followed by Bonferroni *post hoc* testing. Black asterisks: trained distance of DBS/TR versus TR at each time point; grey asterisks: trained distance compared between time points within group. (**E**) Recovery of average BBB scores by group over time compared to pretreatment level (dpi84). BL = post-implantation baseline. *X*-axis: numbers indicate days post-injury (dpi); 3(group) × 11(time) mixed-factorial ANOVA ($P < 0.001$) followed by Bonferroni *post hoc* testing comparing performance at each time point after treatment start with pretreatment performance by group. (**F**) Representative joint trajectories of DBS/TR animal showing step cycle before and after training phase. (**G** and **H**) Development of (**G**) hindlimb (HL) stepping frequency and (**H**) hip height compared to pretreatment level (dpi84) in each group over time. BL1/2 = Baseline before/after electrode implantation; 3(group) × 4(time) mixed-factorial ANOVA ($P < 0.001$) followed by Bonferroni *post hoc* testing comparing performance at each time point after treatment start with pretreatment performance by group. (**I–K**) Recovery rates of (**I**) BBB score, (**J**) stepping frequency and (**K**) hip height compared between groups per period. dpi84–126 = training period. dpi126–154 = retention period; 3(group) × 3(period) mixed-factorial ANOVA ($P < 0.001$) followed by Bonferroni *post hoc* testing comparing change in parameter between groups by period. $^{*}P < 0.05$, $^{**}P < 0.01$, $^{***}P < 0.001$. Data are presented as mean + SD. Scatter represents single animals. (**E**, **G** and **H**) Grey area marks training period. (**H** and **K**) Number of observations <*n* until dpi84 as hip height is unmeasurable until reappearance of ≥1 step cycle.

water (4 cm) providing gravity support to facilitate hindlimb stepping but prevent swimming. A tubing system, open heating bath circulator, laboratory liquid pump and insulating 5 cm polystyrene layer kept water temperature constant at 27 ± 0.9°C. Stimulation was performed with an external stimulator (World Precision Instruments); wires were isolated with hydrophobic silicon oil at the junction to the head plug. Prior to each training cycle, bladder management was performed and individual motor thresholds (50 Hz, 0.5 ms) were evaluated in DBS/TR animals. Each DBS/TR animal underwent three cycles of high-intensity aquatraining with each 10 × 10 s of CNF-DBS-enhanced hindlimb stepping followed by 30 s of rest, resembling interval training. Stimulation intensities from TH to ≤TH +40% unambiguously and reproducibly evoked clearly enhanced hindlimb stepping in 99% of all training

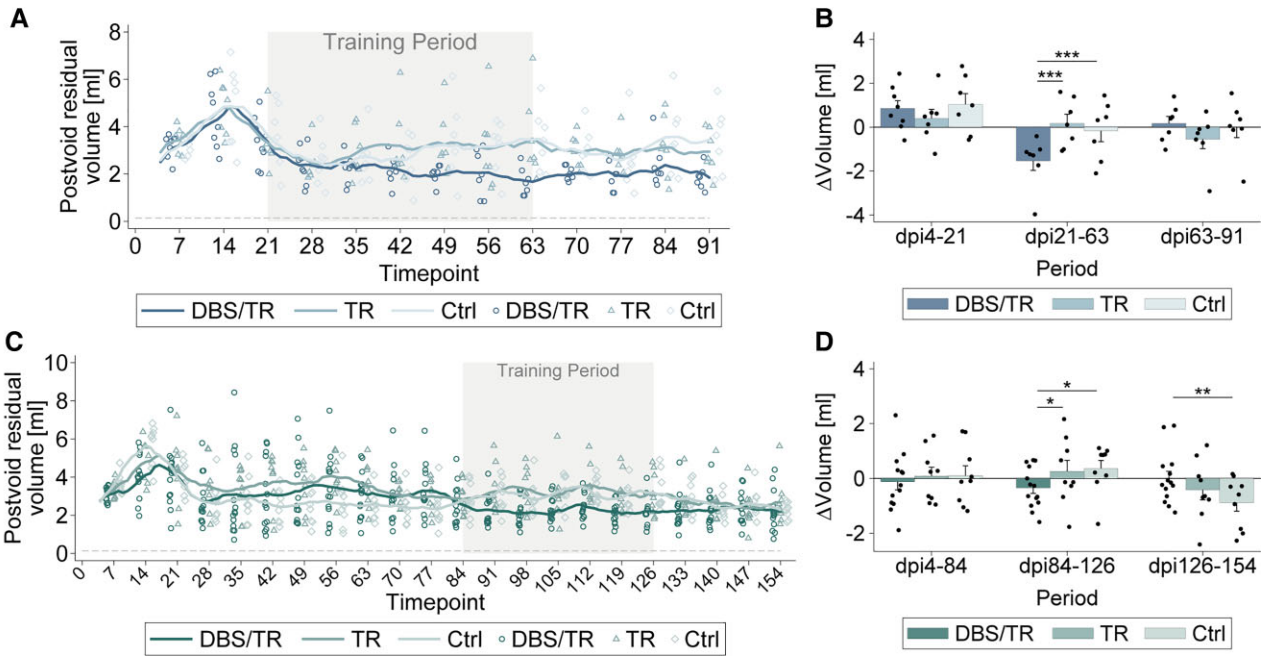

Figure 6 High-intensity locomotor training enabled by repeated CNF-DBS improves lower urinary tract function. (**A**) Development of post-void residual urine volumes over time expressed as moving average (±3 days) by group in subchronic SCI. Control group (Ctrl) = no training ($n = 7$); TR group = training only ($n = 7$); DBS/TR group = training + DBS ($n = 8$). Scatter represents individual animals' moving averages (plotted only on every seventh day to improve readability). (**B**) Intergroup comparison of changes in moving average (±3 days) of post-void residual urine volumes per period: dpi4–21 = recovery period; dpi21–63 = training period; dpi63–91 = retention period. (**C**) Development of post-void residual urine volumes expressed as moving average (±3 days) by group in chronic SCI. Control group = no training ($n = 9$); TR group = training only ($n = 9$); DBS/TR group = training + DBS ($n = 14$). Scatter represents individual animals' moving averages (plotted only on every seventh day to improve readability). (**D**) Intergroup comparison of changes in moving average (±3 days) of post-void residual urine volumes in three phases: dpi4–84 = recovery period; dpi84–126 = training period; dpi126–154 = retention period. (**A** and **C**) Grey dashed line represents intact control value based on Keirstead *et al.*[46] Grey area marks training period. (**B** and **D**) Asterisks indicate significance of Bonferroni *post hoc* test comparing change of post-void residual volumes between groups by period after 3(group) × 3(period) mixed-factorial ANOVA ($P < 0.001$). *$P < 0.05$, **$P < 0.01$, ***$P < 0.001$. Data are presented as mean + SD. Scatter represents single animals. dpi = day post-injury.

stimulations (stimulation intensities: 49.53 ± 11.51 µA in subchronic cohort; 59.59 ± 10.81 µA in chronic cohort). TR animals performed low-intensity aquatraining without stimulation in parallel. Between cycles, animals rested for 1 h. Animals were trained in groups of up to four animals. Colour coding and filming with a wide-angle camera (GoPro Hero6 Black) enabled automated tracking of each animal's training distance (EthoVision XT, Noldus).

Assessment of lower urinary tract function

Post-void residual urine volume is the urine volume remaining in the bladder after voiding due to nervous system dysfunction. Following SCI, bladders were expressed via conscious manual Credé manoeuvre as described previously[51] twice daily and expressed post-void residual volumes were measured (2 decimals). Morning volumes of the subchronic and chronic cohort were analysed, expressed as moving average (±3 days).

Histological analysis

Perfusion and tissue preparation

Animals were euthanized with an intraperitoneal overdose of pentobarbital (300 mg/ml, Streuli Pharma) and transcardially perfused with 200 ml of 1% heparin–Ringer solution (B. Brown Medical Inc), followed by 300 ml of 4% paraformaldehyde (PFA, Sigma Aldrich) solution containing 5% sucrose. Brain and spinal cord were dissected, postfixed in 4% PFA at 4°C for 24 h, and cryoprotected in 30% sucrose solution at 4°C for 3 days. FB-traced brains were embedded in a gelatin-based matrix containing chicken egg albumin that polymerized with glutaraldehyde,[22] minimizing tissue shrinkage and distortion during freezing for accurate reconstruction, and 100-µm thick horizontal vibratome sections were collected on slides (Superfrost, Gerhard Menzel). All other brainstems and spinal cords were embedded in Tissue-Tek O.C.T. (Sakura), cryosectioned coronally (40 µm), collected on-slide or free-floating in 0.1 M PB), and stored at 4°C or −20°C (in antifreeze solution: 300 g glucose, 1000 ml 0.05 M PB, 600 ml ethylene glycol; virus tracing) until further processing.

Lesion size assessment

Nissl-stained (40 µm) lesion sites were manually reconstructed in a 2D T10 spinal cord template (Fig. 2B) based on a spinal cord atlas[45] and neuroanatomical studies[22] using Fiji and Adobe Illustrator CS6. The percentage of spared tissue was calculated for total white matter, grey matter and main motor tracts: corticospinal, rubrospinal, reticulospinal (mesencephalic, pontine, medullary reticulospinal), vestibulospinal tract. Seven rats (subchronic cohort, $n = 6$; chronic cohort, $n = 1$) were excluded retrospectively due to complete lesions.

Immunohistochemistry and analysis

On-slide and free-floating spinal cord sections (40 µm; L2 and L5) were blocked and permeabilized in tris-NaCl blocking buffer (TNB) containing 0.3% Triton X-100 for 60 min at room temperature,

before incubation with primary antibodies (mouse-anti-vGAT, 1:250, Synaptic Systems; rabbit-anti-5HT, 1:2000, ImmunoStar) diluted in TNB containing 0.05% Triton X-100 at 4°C overnight. Sections were washed 3× in 0.1 M PBS for 10 min each, incubated with secondary antibodies (goat-anti-mouse-Cy5, 1:500, Jackson ImmunoResearch; donkey-anti-rabbit-Cy3, 1:500, Jackson ImmunoResearch) for 60 min at room temperature and counterstained with DAPI (1:2000). Sections were washed 2× in 0.1 M PBS and incubated in 0.05 M Tris (pH 8.0) for 10 min each, air-dried overnight at 4°C and coverslipped with fluorescence mounting medium (Mowiol, Merck). Signal specificity was assessed for each marker by primary antibody omission. Imaging was performed using a fluorescent microscope (Axio Scan.Z1, Zeiss; 20×). Microscope and laser parameters were optimized during first imaging and kept constant across all sections. Images were processed using Zen 2 software and exported in TIFF format. Three randomly chosen sections per animal, marker and level (L2, L5) were analysed with Fiji. For vGAT, mean grey values for ventral horn and dorsal grey commissure (lamina X) were measured and averaged after subtracting background value (a.u., arbitrary unit). For 5HT, total axon length (mm) covering ventral horn and lamina X was quantified using AxonTracer (ImageJ)[52] and averaged.

Quantification of retrograde CNF tracing

After imaging of horizontal whole-brain sections (100 µm) using a fluorescent microscope (Axio Scan.Z1, Zeiss; 5×) and verification of the accuracy of injections,[53] images were processed and analysed with Zen 2 and Fiji. Determination of cell count, location and 3D reconstruction was modified from a previous publication.[22] Briefly, the resulting scans were stacked and automatically aligned in Fiji, followed by manual correction if needed. Positions of labelled cells were manually determined and put into reference to predefined anatomical landmarks marked on the midline and corresponding projection at the border of the brain: rostral end of olfactory bulb, anterior commissure, red nucleus, cranial nerve VII, decussation of pyramids. Each cell's position was computationally corrected for mediolateral and rostrocaudal distortions of sections using STATA statistical software, version 14 (StataCorp, College Station, TX), and fitted into a standard rat brain model.

Quantification of anterograde CNF tracing

Every third brainstem section (40 µm) containing the NRG and the CNF, respectively, was counterstained with DAPI (1:2000 in PBS) and coverslipped using Mowiol after drying. Brainstem sections were imaged using a fluorescent microscope (Axio Scan.Z1, Zeiss; NRG: 20×; CNF: 10×) with constant parameters. Images were processed using Zen 2 software, Fiji and Adobe Illustrator CS6. After verification of successful and anatomically accurate tracer injection confined to the CNF[53] (one animal excluded), labelled CNF fibres in the NRG were manually reconstructed over a distance of 3 mm and the NRG area covered by fibres was calculated (pixels). To correct for interanimal variability in tracing efficiency, absolute counts were normalized to the total number of labelled cells in the CNF (a.u.).

Statistical analysis

Data processing, statistical analysis and preparation of graphs was performed in STATA statistical software, version 14 (StataCorp, College Station, TX). Figures were generated with Adobe Illustrator CC 2019. Animals and groups are consistently colour-coded. Animals were number-coded and investigators blinded to groups, conditions and time points until the end of data analysis, except for data acquisition and analysis involving directly visible effects of CNF-DBS on behaviour. No statistical outliers were excluded. Bars indicate means + SD, except for Fig. 1G (means + SEM). Written data are shown as means ± SD. Sample sizes were chosen based on previous experiments using similar animal models and the maximal number of animals that can be included in training experiments; no statistical method was used for sample size calculation. Behavioural data of acute stimulation experiments: for comparison of more than two groups or conditions, one-way repeated-measures ANOVA followed by Bonferroni *post hoc* testing was performed; to detect differences between conditions or within groups over time, two-way repeated-measures ANOVA followed by Bonferroni *post hoc* testing was performed. Kinematic data and BBB scoring of acute DBS experiments are shown for the left hindlimb ipsilateral to electrode implantation (comparable results of right hindlimb). Recovery of motor function over time with long-term CNF-DBS-enhanced training was analysed by mixed-factorial ANOVA followed by Bonferroni *post hoc* testing for multiple comparison comparing each parameter at each time point after treatment start with pretreatment performance by group. To quantify improvements of motor and bladder function between crucial time points, we calculated the effect size (change of parameters between key time points marking periods) and performed mixed-factorial ANOVAs followed by Bonferroni *post hoc* testing for multiple comparisons between all groups by period. BBB data were analysed using parametric statistics as reported previously[50,54] and discussed by Scheff *et al.*[55] BBB analysis is depicted for right hindlimb (results are mirrored for left hindlimb); kinematic analysis was performed with mean across both hindlimbs due to symmetric lesion morphology and comparable results for both hindlimbs. Neuroanatomical data were analysed by one-way (group) ANOVA followed by Bonferroni *post hoc* test. *P*-values after ANOVA type in figure legends indicate significance of model (two-way, mixed-factorial) or parameters of interest (one-way). *P*-values in text and asterisks in figures indicate significance of Bonferroni *post hoc* tests ($^{*}P < 0.05$, $^{**}P < 0.01$, $^{***}P < 0.001$).

Data availability

The data that support the findings of this study are available from the corresponding author, upon reasonable request.

Results

Safety window of CNF stimulation ensuring context-specific locomotor control

We assessed the eventual loss of coordinated motion control in a series of behavioural tasks without (baseline) and with CNF stimulation. Speed and pattern of over-ground locomotion during CNF-DBS were intensity-dependent (Fig. 1A–D). Speed increased gradually from TH intensity (0.83 ± 0.08 m/s at TH versus 0.65 ± 0.05 m/s at baseline; Fig. 1A) and exceeded baseline speed about 4-fold at TH +100%. Hindlimb stepping frequency increased significantly from TH +30% (6.09 ± 0.47 Hz, $P < 0.001$; Fig. 1B) compared to baseline (4.12 ± 0.25 Hz). Unilateral CNF-DBS initiated coordinated

quadrupedal locomotion with symmetric stepping of left and right limbs: all animals showed alternating hindlimb stepping (synchronization of 4.07 ± 2.17% at baseline) at low-intensity stimulation (<TH +40%) and a gradual transition to trotting and galloping with left–right synchronization of stepping at higher strengths (48.48 ± 2.41% with TH +100%; $P < 0.001$; Fig. 1C and D). This was paralleled by increased forelimb frequency from TH +30% ($P < 0.05$) and inter-forelimb synchronization from TH + 50% ($P < 0.001$; data not shown). A shift from alternating hindlimb strokes (synchronization of 2.98 ± 1.16% at baseline, Fig. 1E) towards a gradual synchronization resulting in gallop-like movements with TH +50% (20.83 ± 16.09%; $P < 0.001$) and above (46.28 ± 4.26% at TH +100%, $P < 0.001$) was also observed during swimming. At TH +80% animals submerged under the surface to gallop at the bottom of the experimental setup (−9.29 ± 6.58 cm below surface at TH +90% versus +0.74 ± 0.32 cm above surface at baseline; $P < 0.001$; Fig. 1F). In the place preference task, animals exhibited a clear preference for darkness until TH +100% (Fig. 1G), despite moving at high speeds at high intensities. At very high stimulation intensities CNF-DBS started to interfere with animals' natural place preference and significantly increased the relative time spent in the bright zone at TH +110% ($P < 0.05$) and TH +120% ($P < 0.01$). Nevertheless, the majority of time was still spent in the dark zone. High speeds of movements are frequently associated with reduced sensory responsiveness and dexterity. We therefore tested the influence of CNF-DBS on obstacle avoidance capability and speed control, and compared delay times prior to obstacle crossing at each stimulation intensity with baseline (3.83 ± 0.87 s; Fig. 1H, black asterisks). At all intensities up to TH +60%, animals remained able to stop prior to obstacle crossing, reflected by insignificantly shorter delay times ($P > 0.05$) compared to baseline (significantly longer than 0 s, $P < 0.001$, grey asterisks). The delay significantly decreased with stimulation strengths ≥TH +80%, indicating loss of obstacle avoidance capability (0.57 ± 1.12 s at TH +80%; $P < 0.001$ versus baseline; $P > 0.05$ versus 0 s). The ability to adapt speed to environmental conditions persisted at all stimulation intensities with significantly lower overall speeds in presence of an obstacle ($P < 0.05$ at TH; $P < 0.001$ at suprathreshold intensities; Fig. 1I).

Main input structures of the CNF

Retrograde FB tracing of the left CNF in intact animals labelled a variety of sensory and motor input structures throughout the brain (Fig. 1J and K). The greatest number of neurons projecting bilaterally to the CNF was found in the periaqueductal grey, the inferior colliculus, the PPN and the nucleus raphe. Strong ipsilateral projections came from the thalamic nuclei, and the secondary somatosensory, visual and retrosplenial cortex. Strong commissural projections were present between left and right CNF.

Locomotor effects of CNF-DBS in spinal cord-injured rats depend on post-injury time window

We performed a timeline experiment to study the therapeutic window and optimal timing of CNF-DBS (Fig. 2A) to improve locomotion in rats with large T10 injuries, sparing only the ventromedial white matter bilaterally (Fig. 2B and C). Animals underwent weekly locomotion assessment without (baseline) and with CNF-DBS at increasing stimulation intensities on post-injury Days 3, 7, 14, 21, 28 and 35, and immediate effects of CNF-DBS on hindlimb stepping were analysed. Fibre sparing in the reticulospinal tract was 20 ± 15% (Fig. 2C). All animals had paraplegic hindlimbs after injury and showed only limited recovery over time, a condition resembling a human SCI severity of ASIA B to severe C. Acutely after injury, CNF-DBS induced minor acceleration of locomotor speed, driven entirely by forelimb activation, in all animals (Fig. 2D; $P < 0.001$). However, no hindlimb responses were elicited by CNF-DBS in the first 7 days (Fig. 2E and F; 0 ± 0 Hz; $P > 0.05$). Fourteen days after injury, some animals exhibited non-functional hindlimb movements upon CNF-DBS (Fig. 2G; $P > 0.05$). On dpi21 (Fig. 2H) and dpi28 (Fig. 2I), CNF-DBS elicited and significantly enhanced hindlimb stepping frequency in the majority of animals with ≥TH +30%. Five weeks after injury, suprathreshold CNF-DBS re-established and significantly improved hindlimb stepping in all animals with bilateral, ventral white matter sparing (Fig. 2J, $P < 0.001$ with ≥TH +30%). A detailed analysis of key parameters of hindlimb stepping at dpi35 is shown in Supplementary Fig. 3. Subthreshold stimulation (TH −10%) did not affect any parameter at any time point. BBB scoring revealed plegic or highly paretic hindlimbs until dpi21 (Fig. 2K–M). Five weeks after injury, animals achieved significantly better walking ability during CNF-DBS at all stimulation intensities (Fig. 2N; $P < 0.01$ at TH; $P < 0.001$ >TH) including rhythmic hindlimb stepping with full range of motion (BBB 7–8) and weight-bearing capacity (BBB of 9–11; representative joint angle kinetics in Fig. 2O and P).

Therapeutic window of CNF-DBS is mirrored in anatomical plasticity of CNF projection to the NRG

Our results show a complete absence of functional hindlimb responses to CNF-DBS 3–14 days after subtotal spinal cord transection followed by a progressive improvement of stimulation-induced hindlimb locomotion 3–5 weeks after injury. To identify potential neuroanatomical correlates, we quantified the output of the left CNF to the ipsilateral NRG (Fig. 3) in intact and injured rats (dpi 7, dpi14, dpi35; Fig. 3A and B) using a fluorescent anterograde viral tracer. An ipsilateral predominance of CNF-NRG connections was present (Fig. 3C and D), with only very few projections detectable to the contralateral NRG (quantification not shown). Thirty-five days after injury, the density of CNF fibres in the ipsilateral NRG had increased more than 2.5-fold ($P < 0.01$ versus dpi14; Fig. 3E). No significant difference in fibre counts was observed between the intact situation, dpi7 and dpi14.

Enhanced and persistent gait recovery with CNF-DBS-enabled training in subchronic spinal cord injury

To reveal the therapeutic potential of repeated CNF-DBS as an enhancer of hindlimb step training and functional recovery in subchronic animals, we randomly allocated animals with severe incomplete hindlimb paralysis to three 6-week rehabilitation schedules (Fig. 4A; dpi21–dpi63). Three weeks after >90% thoracic cord transection, animals performed either (i) daily high-intensity wading in shallow water (aquatraining) accompanied by suprathreshold CNF-DBS (DBS/TR group; $n = 8$); (ii) daily aquatraining without stimulation (TR group; $n = 7$); or (iii) were observed for spontaneous recovery without training (Contol group; $n = 7$). Lesion sizes were comparable between groups [on average <10% white matter sparing, Fig. 4B and C; $P > 0.05$]. Stimulated animals waded significantly greater distances (Fig. 4D; $P < 0.001$) than non-stimulated animals (138.02 ± 18.23 m versus 40.05 ± 21.25 m in training Week 3). Distances significantly increased with time in the DBS/TR group (Week 6 versus 1, $P < 0.001$). The fraction of spared reticulospinal

fibres showed a weak positive correlation with the trained distance in DBS/TR animals only (Supplementary Fig. 4A and B). All groups exhibited very low BBB scores initially (Fig. 4E), with minimal spontaneous recovery within the first 3 weeks (dpi21). Seven weeks after injury (dpi49) non-stimulated animals (TR, Control) reached a comparable functional plateau insignificantly better compared to their pretraining performance. In contrast, CNF-DBS significantly improved hindlimb stepping during the training period, resulting in mean BBB values of 11 ± 3.4 (dpi63 versus dpi21; $P < 0.001$) compared to 6.1 ± 2 in the TR group (BBB of 10 indicates recovery of antigravitational strength). After discontinuation of CNF-DBS at dpi63, hindlimb function remained significantly better than before training ($P < 0.001$; versus dpi21) and was stable for at least 4 weeks until dpi91 (DBS/TR: 10.5 ± 3.1; TR: 5.6 ± 1.9). Kinematic analysis of walking performance at key time points revealed marked improvements in stepping frequency with CNF-DBS over time ($P < 0.01$, dpi42 versus dpi21; $P < 0.001$, dpi63 versus dpi21; Fig. 4F and G). This beneficial effect persisted beyond the training phase (dpi91 versus dpi21; $P < 0.001$). Without DBS, recovery was insignificant at all time points ($P > 0.05$, TR and Control). Antigravitational strength (Fig. 4H) was heavily impaired after SCI, and since determining hip height requires at least one step cycle, it was unmeasurable in some animals before dpi42. All animals regained stepping capacity during training period and hip height significantly recovered in the DBS/TR group ($P < 0.01$). Hip height did not improve in non-stimulated groups ($P > 0.05$). We additionally performed an intergroup comparison of the change in performance between key time points (dpi21–dpi63 and dpi63–dpi91; Fig. 4I–K). Compared to non-stimulated groups, DBS/TR animals regained significantly more stepping quality (Fig. 4I; $P < 0.001$), stepping frequency (Fig. 4J; $P < 0.001$) and hip height (Fig. 4K; $P < 0.001$) during training. Recovered BBB scores and stepping frequency persisted beyond discontinuation of training ($P > 0.05$). Recovered hip height dropped insignificantly after discontinuation of CNF-DBS (Fig. 4H and K). Neither the trained distance nor the fraction of spared reticulospinal fibres significantly correlated with improvements in BBB scores in DBS/TR and TR animals (Supplementary Fig. 4C–F). Control animals' recovery was not correlated with the fraction of spared reticulospinal fibres (Supplementary Fig. 4G). CNF-DBS also improved hindlimb kinematics immediately upon stimulation in the chronic injury phase (dpi91; Supplementary Fig. 5A–D). Despite chronic and frequent stimulation, CNF-DBS remained efficient at gradually increasing locomotor speed throughout the entire study period (Supplementary Fig. 6A–C), even though motor thresholds increased significantly ($P < 0.001$ on dpi63 and dpi91 versus dpi21; data not shown). Post-mortem, *ex-situ* magnetic resonance images (7 T) demonstrate preservation of tissue integrity (Supplementary Fig. 6G–J). Anatomically, we found a significantly lower expression of vGAT in stimulated animals compared to non-trained animals in ventral horn and lamina X of sublesional levels L2 and L5 (Fig. 4L; $P < 0.05$ in ventral horn of L2, $P < 0.01$ in ventral horn of L5 and lamina X of L2 and L5). Significantly lower vGAT levels were also found in TR animals compared to non-trained animals in lamina X of L2 and L5 ($P < 0.05$) and ventral horn of L5 ($P < 0.01$). No significant differences were observed between both training groups ($P > 0.05$) in any region or level. A significantly higher serotoninergic fibre length was evident in ventral horn of L2 and L5 of DBS-treated animals compared to control animals ($P < 0.05$; Fig. 4M). Serotoninergic fibre length was significantly higher in TR animals compared to control animals in ventral horn of L5 ($P < 0.05$).

Long-term CNF-DBS can reinitiate and drive gait recovery in chronic spinal cord injury

We additionally investigated the capability of repeated CNF-DBS to enable step training and improve ambulation in chronic SCI animals (Fig. 5A) that had reached a plateau with stagnating recovery. Twelve weeks after severe, >90% T10 SCI and limited spontaneous recovery, a DBS/TR group underwent CNF-DBS-induced high-intensity aquatraining daily for 6 weeks ($n = 14$). Two groups performed either aquatraining without stimulation (TR, $n = 9$) or no training (Control, $n = 9$). Lesion sizes were comparable (on average <10% white matter sparing; Fig. 5B and C; $P > 0.05$). At all time points, DBS/TR animals covered significantly ($P < 0.001$) greater training distances (140.58 ± 26.39 m versus 13.28 ± 8.95 m in Week 3; Fig. 5D), and distances of DBS/TR increased over time ($P < 0.05$), with a positive correlation with the fraction of spared reticulospinal fibres (Supplementary Fig. 4A). Seven weeks after injury, spontaneous motor recovery reached a plateau with mean BBB scores of 7–9 in all groups (dpi49; Fig. 5E). While BBB scores remained stable thereafter in TR and Control groups ($P > 0.05$), 6 weeks of CNF-DBS-enabled training significantly improved hindlimb stepping ($P < 0.05$ on dpi126) compared to the pretreatment level (dpi84). This effect remained and even increased slightly ($P < 0.01$) beyond the training phase, with recovery of rhythmic hindlimb stepping and antigravitational strength reflected by BBB scores of 8–19. Compared to the pretraining performance, absolute values of stepping frequency and hip height did not change significantly over time in any group (Fig. 5F–H; $P > 0.05$; hip height was unmeasurable in some animals until reappearance of step cycles at dpi84). However, differential recovery patterns become obvious when comparing changes during the training and retention period between groups (Fig. 5I–K): CNF-DBS-initiated step training significantly enhanced improvements in BBB scores (Fig. 5I), stepping frequency (Fig. 5J) and hip height (Fig. 5K; $P < 0.001$ DBS/TR versus TR and Control). Improvements in BBB scores were stable (dpi126–154; $P > 0.05$; Fig. 5I). The beneficial effects on stepping frequency and hip height vanished with the discontinuation of training (dpi126–154; Fig. 5J and K). Nevertheless, DBS/TR animals significantly outperformed both non-stimulated groups with respect to recovery during the training period. In DBS/TR animals, training distances and fraction of spared reticulospinal fibres were positively correlated with the extent of locomotor recovery (Supplementary Fig. 4C and E). TR and control animals did not show correlations (Supplementary Fig. 4D, F and G). CNF-DBS immediately improved hindlimb function upon stimulation (Supplementary Fig. 5E–H) even at a very chronic post-injury stage (dpi154). Even though motor thresholds increased significantly after 6 weeks of repeated CNF-DBS ($P < 0.001$ on dpi126 and dpi154 versus dpi84; data not shown), CNF-DBS remained efficacious, resulting in intensity-dependent, significant increases in overall speed upon stimulation in the open field throughout the entire study period (Supplementary Fig. 6D–F). Structure of tissue surrounding the electrode tip was preserved, as shown by 7 T MRI (Supplementary Fig. 6G–J) and Nissl-staining (Supplementary Fig. 6K and L). Perifocal gliosis (GFAP, Supplementary Fig. 6M and N) and microglia activation (Iba1, Supplementary Fig. 6O and P) was low.

CNF-DBS-induced locomotor training improves lower urinary tract function

We analysed the influence of CNF-DBS-enabled locomotor training on lower urinary tract function as secondary readout (Fig. 6). All animals exhibited flaccid bladder paralysis acutely after injury with insufficient emptying, resulting in high post-void residual morning

volumes (Fig. 6A and C). Residual volumes peaked 14 days after injury. After 2 weeks of DBS-enabled training initiated in early chronic SCI (dpi35), post-void residuals decreased in stimulated animals (Fig. 6A) and groups exhibited large, persisting differences after 4 weeks of training (dpi49, DBS/TR: 2.00 ± 0.38 ml; TR: 3.24 ± 1.33 ml; Control: 3.23 ± 1.68 ml). Intergroup comparison of post-void residual volume changes per period (Fig. 6B) showed that CNF-DBS-enabled training markedly improved bladder emptying ($P < 0.001$). After training discontinuation, bladder emptying remained better in CNF-DBS-treated animals. CNF-DBS in late chronic SCI resulted in consistently lower post-void residual urine volumes during the training period (dpi105, DBS/TR: 2.27 ± 0.63 ml; TR: 3.07 ± 1.33 ml; Control: 3.23 ± 0.77 ml; Fig. 6C), and residual volumes improved significantly more with CNF-DBS (Fig. 6D; $P < 0.05$). Interestingly, post-void residual volumes of TR and control animals decreased in the retention period, resulting in similar volumes in all chronic groups at very late time points after injury (>dpi140; Fig. 6C and D).

Discussion

We first identified the range of stimulation strengths ensuring safe and efficacious application of CNF-DBS in intact rats. We then applied CNF-DBS to spinal cord-injured animals either in the acute, subchronic or chronic phase. Marked immediate effects on locomotion were seen in the subchronic and chronic phases, emphasizing the significance of proper timing of treatment initiation. Repeated, daily CNF stimulation enabled high-intensity hindlimb training and resulted in restored functional stepping and improved long-term motor recovery.

The MLR–reticulospinal system can be modulated in an intensity dependent manner by DBS,[10,22,39] and unilateral stimulation is sufficient to induce quadrupedal locomotion with proper coupling of left and right limbs due to reciprocal and bilateral connections between long-distance descending spinal neurons, reticulospinal tract and spinal commissural interneurons.[56–59] Stimulation intensities up to 40–60% above motor threshold induced locomotion with preserved adaptability to contextual cues, which bears great relevance for the safe and successful application of CNF-DBS in human patients. Adaptation to changing contexts and environments, e.g. walking on uneven ground or approaching obstacles, requires higher brain control.[2,60,61] We identified and confirmed a variety of bilateral and unilateral input structures to the CNF[12,40,62] (co-labelling of PPN inputs cannot be fully excluded). Inferior[63] and superior colliculus,[64] secondary somatosensory cortex or retrosplenial cortex[65] integrate a variety of sensory inputs and send output signals to downstream locomotor control centres, including the MLR.[60,66] Overwriting these suprabulbar, modulatory inputs by external stimulation of the CNF, leading to reduced locomotor control, was only observed at very high intensities (>TH +60–80%).

Our results suggest the presence of a critical time window for therapeutic efficacy of CNF-DBS after SCI. We hypothesize that CNF-DBS activated the sparse, remaining fibres, probably mainly reticulospinal, projecting to the lumbar cord below the severe thoracic injuries, which destroyed >90% of the spinal cord cross-section. With these lesions, on average, 20 ± 15% of the reticulospinal tract fibres were preserved. They triggered coordinated activity in local CPGs and enhanced speed and strength of hindlimb stepping in subchronic and chronic animals immediately upon initiation of CNF-DBS. Importantly, however, CNF-DBS did not elicit hindlimb motion in the acute post-injury phase. In contrast, direct sublesional spinal cord stimulation has been shown to activate spinal motor circuits 7 days after injury.[28] The time lag of hindlimb responsiveness to CNF-DBS was not related to areflexia and loss of excitability due to early spinal shock, as hindlimb stretch reflexes had reappeared since dpi3 in all animals (data not shown).[47,67] However, a temporally correlated increased density of CNF projections to the ipsilateral NRG was evident. Spared reticulospinal fibres have been shown to undergo compensatory sprouting in the lumbar spinal cord,[68] and severed fibres rearrange and form contacts onto propriospinal relays to bypass the site of injury[69] with a comparable time course of 3–5 weeks after injury. We hypothesize that sprouting and arborization of CNF fibres projecting to reticulospinal nuclei and of the severed reticulospinal tracts are key for locomotion induction by CNF-DBS. CNF-DBS markedly improved or re-established hindlimb stepping in all animals with bilateral, ventral white matter sparing, even in the case of >95% spinal cord cross-sectional tissue destruction. Fibre sparing exclusively within the ipsilateral lateral funiculus or the ventral funiculus contralateral to stimulation did not allow stepping initiation upon CNF-DBS. In line with the literature, CNF-DBS-initiated stepping depends on spared ipsilateral ventromedial fibres.[14,22,70] This criterion should be considered in the selection of patients for future clinical applications and when determining the side of electrode implantation. However, due to its dispersed rather than focal course in the spinal cord white matter including the periphery,[71] the reticulospinal system is likely to be partially spared after anatomically incomplete SCI in humans.[15] In most clinically complete injuries small amounts of white matter remain intact, cross the level of injury[15–17] and retain their capability for signal transmission;[72,73] such lesions have sometimes been referred to as discomplete.[74] Sparing and contribution of the reticulospinal tract to motor recovery have been demonstrated in patients with motor complete and incomplete SCI.[75,76] Ventral tissue bridges at the lesion site are frequently detectable with conventional MRI, even in clinically motor complete patients categorized as AIS A or B,[77–80] and correlate to electrophysiological measurements and functional outcome.[77,79] Although CNF-DBS is not a therapeutic option for anatomically complete SCI, it can be considered for the majority of SCI patients with functionally incomplete and functionally complete, anatomically incomplete (discomplete) SCI. These patients can be identified and stratified by conventional MRI together with electrophysiological measurements and clinical assessments. Epidural spinal cord stimulation has yielded promising results in studies on motor complete spinal cord-injured patients,[21,30,81] yet a relevant proportion of motor complete patients responding to epidural stimulation has been suggested to be anatomically incomplete,[78,80] and thus the contribution of supraspinal inputs transmitted via spared, dormant fibres at the lesion site to observed volitional motor output with epidural stimulation cannot be excluded.

Various experimental neuromodulatory approaches to enhance training efficacy are offered to select spinal cord-injured patients in clinical studies worldwide.[82–84] However, conventional physical training is so far still the only widely and routinely applied treatment to promote functional recovery after motor incomplete SCI in human patients.[85] Improvements achieved with classical neurorehabilitation appear in the subchronic post-injury phase and reach a plateau in the chronic period when the recovery potential strongly decreases.[86–89] The resulting walking ability is limited.[1] In our study, we modelled these two crucial phases of motor recovery after severe, incomplete SCI in rats: early/subchronic and late/

chronic. In all animals that did not undergo CNF-DBS, motor improvements stagnated at a low functional level around 7 weeks after trauma. This time course is in line with the experimental literature[90] and comparable to clinical observations.[88] CNF-DBS-enabled high-intensity aquatraining, however, substantially improved ambulation in both subchronic and chronic SCI, resulting in recovered antigravitational strength and coordinated, rhythmic hindlimb stepping. Extent and persistence of regained functions were most pronounced after an early start of high-intensity training before a functional plateau had been reached. Maintenance of a higher level of motor function for weeks beyond the stimulation period suggests long-term changes in CNS circuitry as a result of stimulation-enabled high-intensity training. Persisting gait improvement has also been demonstrated after locomotor training supported by epidural stimulation and serotonergic agonists in spinal cord-injured rats.[19] Combining PPN stimulation with training enhanced by epidural stimulation and serotonin agonists has yielded synergistic locomotor effects in rats with incomplete thoracic spinal cord contusions.[91] However, acute PPN stimulation alone was ineffective to promote locomotion, which might further emphasize the CNF as the relevant target for therapeutic DBS after SCI.[38–41,92]

Spinal cord trauma also impairs bladder control, significantly reducing quality of life.[93] The best available routine treatment today is catheterization. Our findings indicate a beneficial influence of CNF-DBS-enhanced locomotor training on micturition efficiency, resulting in lower post-void residual urine volumes. Direct projections from the CNF[94] to the pontine micturition centre (PMC, Barrington nucleus) might be the corresponding anatomical correlate. Additionally, CNF and PPN are connected bidirectionally,[40] and PPN and PMC are in close proximity in humans and rodents[95] with PMC dendrites terminating near the PPN.[96] Anecdotally, we observed an inhibition of CNF-DBS-induced stepping when bladders were full in both intact and injured animals. Locomotor training-related improvements in autonomic function were also observed clinically.[97] Effects of CNF-DBS are encouraging, but need to be studied in more detail in human subjects. The comparison to other emerging neurostimulation approaches targeting peripheral nerves or the spinal cord will be interesting. Sacral root stimulation has been used for years to improve micturition in SCI patients; however, is not widely applied due to its complexity.[98] Tibial nerve stimulation has been reported to be effective in treating neuropathic overactive bladder preclinically[99] and clinically.[100,101] In addition to promoting motor recovery, epidural stimulation has improved bladder function in several cases.[102–104] While the exact mechanisms driving the positive impact of training and neurostimulation on motor and bladder function are poorly understood, effects seem reproducible. Future clinical studies will show whether focal stimulation at the brainstem or spinal level can positively affect multiple systems simultaneously and long term. This would have enormous impact on the quality of life of SCI patients.

Improving functional recovery is a big challenge after SCI, and CNF-DBS may be a promising novel therapeutic approach for this purpose. CNF-DBS is safe with careful selection of stimulation parameters and due to a projection pattern via multiple downstream relay structures, unilateral, technically relatively simple stimulation of the CNF is sufficient to elicit complex locomotor responses. Treatment initiation in the early, subchronic phase after injury is more efficacious than in the fully chronic phase, and high-intensity training is crucial for long-term motor improvements that persist beyond the discontinuation of training. The effect of CNF-DBS depends on spared reticulospinal fibres and thus patients need to be selected accordingly in ongoing[43] and future clinical trials.

Acknowledgements

We would like to thank Martin Wieckhorst, Hansjörg Kasper and Stefan Giger (University of Zurich) for their great support in technical matters. We also thank Dr Anna Stepien (University of Zurich) for assistance in the preparation of electrodes and Dr Mark-Aurel Augath (University of Zurich and ETH Zurich) for performing *ex-vivo* post-mortem magnetic resonance scans. Imaging was performed with support of the Center for Microscopy and Image Analysis of the University of Zurich.

Funding

Financial support was provided by the Spinal Cord Consortium of the Christopher and Dana Reeve Foundation, a project grant from the Wings for Life Spinal Cord Research Foundation (WFL-CH-30/17), a project grant from the 'Forschungskredit Candoc' of the University of Zurich (FK-17-035) and a project grant from the Foundation for Research in Science and the Humanities at the University of Zurich (STWF-19-011). Funding sources had no influence on design, conduct, analysis and reporting of this research.

Competing interests

The authors report no competing interests.

Supplementary material

Supplementary material is available at *Brain* online.

References

1. Dietz V, Schwab ME. From the rodent spinal cord injury model to human application: Promises and challenges. *J Neurotrauma*. 2017;34:1826–1830.
2. Kiehn O. Decoding the organization of spinal circuits that control locomotion. *Nat Rev Neurosci*. 2016;17:224–238.
3. Grillner S. Biological pattern generation: the cellular and computational logic of networks in motion. *Neuron*. 2006;52:751–766.
4. Kiehn O. Locomotor circuits in the mammalian spinal cord. *Annu Rev Neurosci*. 2006;29:279–306.
5. Grillner S, Wallén P. Central pattern generators for locomotion, with special reference to vertebrates. *Annu Rev Neurosci*. 1985;8:233–261.
6. Ryczko D, Dubuc R. The multifunctional mesencephalic locomotor region. *Curr Pharm Des*. 2013;19:4448–4470.
7. Skinner RD, Garcia-Rill E. The mesencephalic locomotor region (MLR) in the rat. *Brain Res*. 1984;323:385–389.
8. Shik ML, Severin FV, Orlovski? GN. [Control of walking and running by means of electric stimulation of the midbrain]. *Biofizika*. 1966;11:659–666.
9. van der Zouwen CI, Boutin J, Fougère M, *et al*. Freely behaving mice can brake and turn during optogenetic stimulation of the mesencephalic locomotor region. *Front Neural Circuits*. 2021;15:639900.
10. Cabelguen J-M, Bourcier-Lucas C, Dubuc R. Bimodal locomotion elicited by electrical stimulation of the midbrain in the

salamander *Notophthalmus viridescens*. *J Neurosci*. 2003;23:2434–2439.
11. Garcia-Rill E, Skinner RD. The mesencephalic locomotor region. II. Projections to reticulospinal neurons. *Brain Res*. 1987; 411:13–20.
12. Steeves JD, Jordan LM. Autoradiographic demonstration of the projections from the mesencephalic locomotor region. *Brain Res*. 1984;307:263–276.
13. Shefchyk SJ, Jell RM, Jordan LM. Reversible cooling of the brainstem reveals areas required for mesencephalic locomotor region evoked treadmill locomotion. *Exp Brain Res*. 1984;56: 257–262.
14. Noga BR, Kriellaars DJ, Jordan LM. The effect of selective brainstem or spinal cord lesions on treadmill locomotion evoked by stimulation of the mesencephalic or pontomedullary locomotor regions. *J Neurosci*. 1991;11:1691–1700.
15. Kakulas BA. A review of the neuropathology of human spinal cord injury with emphasis on special features. *J Spinal Cord Med*. 1999;22:119–124.
16. Taccola G, Sayenko D, Gad P, Gerasimenko Y, Edgerton VR. And yet it moves: Recovery of volitional control after spinal cord injury. *Prog Neurobiol*. 2018;160:64–81.
17. Dimitrijevic MR, Kakulas BA. Spinal cord injuries, human neuropathology and neurophysiology. *Acta Myol*. 2020;39:353–358.
18. Hubli M, Dietz V. The physiological basis of neurorehabilitation—Locomotor training after spinal cord injury. *J Neuroeng Rehabil*. 2013;10:5.
19. Asboth L, Friedli L, Beauparlant J, *et al*. Cortico-reticulo-spinal circuit reorganization enables functional recovery after severe spinal cord contusion. *Nat Neurosci*. 2018;21:576–588.
20. Wenger N, Moraud EM, Gandar J, *et al*. Spatiotemporal neuromodulation therapies engaging muscle synergies improve motor control after spinal cord injury. *Nat Med*. 2016;22:138–145.
21. Rejc E, Angeli CA, Bryant N, Harkema SJ. Effects of stand and step training with epidural stimulation on motor function for standing in chronic complete paraplegics. *J Neurotrauma*. 2017;34:1787–1802.
22. Bachmann LC, Matis A, Lindau NT, Felder P, Gullo M, Schwab ME. Deep brain stimulation of the midbrain locomotor region improves paretic hindlimb function after spinal cord injury in rats. *Sci Transl Med*. 2013;5:208ra146.
23. Inanici F, Samejima S, Gad P, Edgerton VR, Hofstetter CP, Moritz CT. Transcutaneous electrical spinal stimulation promotes long-term recovery of upper extremity function in chronic tetraplegia. *IEEE Trans Neural Syst Rehabil Eng*. 2018; 26:1272–1278.
24. Sayenko DG, Rath M, Ferguson AR, *et al*. Self-assisted standing enabled by non-invasive spinal stimulation after spinal cord injury. *J Neurotrauma*. 2019;36:1435–1450.
25. Gerasimenko YP, Lu DC, Modaber M, *et al*. Noninvasive reactivation of motor descending control after paralysis. *J Neurotrauma*. 2015;32:1968–1980.
26. Hofstoetter US, Krenn M, Danner SM, *et al*. Augmentation of voluntary locomotor activity by transcutaneous spinal cord stimulation in motor-incomplete spinal cord-injured individuals. *Artif Organs*. 2015;39:E176–E186.
27. Herman R, He J, D'Luzansky S, Willis W, Dilli S. Spinal cord stimulation facilitates functional walking in a chronic, incomplete spinal cord injured. *Spinal Cord*. 2002;40:65–68.
28. Courtine G, Gerasimenko Y, Van Den Brand R, *et al*. Transformation of nonfunctional spinal circuits into functional states after the loss of brain input. *Nat Neurosci*. 2009;12: 1333–1342.
29. Angeli CA, Edgerton VR, Gerasimenko YP, Harkema SJ. Altering spinal cord excitability enables voluntary movements after chronic complete paralysis in humans. *Brain*. 2014;137(Pt 5): 1394–1409.
30. Gill ML, Grahn PJ, Calvert JS, *et al*. Neuromodulation of lumbosacral spinal networks enables independent stepping after complete paraplegia. *Nat Med*. 2018;24:1677–1682.
31. Calvert JS, Grahn PJ, Strommen JA, *et al*. Electrophysiological guidance of epidural electrode array implantation over the human lumbosacral spinal cord to enable motor function after chronic paralysis. *J Neurotrauma*. 2019;36:1451–1460.
32. McPherson JG, Miller RR, Perlmutter SI. Targeted, activity-dependent spinal stimulation produces long-lasting motor recovery in chronic cervical spinal cord injury. *Proc Natl Acad Sci USA*. 2015;112:12193–12198.
33. Hartmann CJ, Fliegen S, Groiss SJ, Wojtecki L, Schnitzler A. An update on best practice of deep brain stimulation in Parkinson's disease. *Ther Adv Neurol Disord*. 2019;12:1756286419838096.
34. Mazzone P, Lozano A, Stanzione P, *et al*. Implantation of human pedunculopontine nucleus: A safe and clinically relevant target in Parkinson's disease. *Neuroreport*. 2005;16:1877–1881.
35. Moro E, Hamani C, Poon YY, *et al*. Unilateral pedunculopontine stimulation improves falls in Parkinson's disease. *Brain*. 2010; 133(Pt 1):215–224.
36. Chang SJ, Cajigas I, Guest JD, *et al*. MR Tractography-based targeting and physiological identification of the cuneiform nucleus for directional DBS in a Parkinson's disease patient with levodopa-resistant freezing of gait. *Front Hum Neurosci*. 2021;15:676755.
37. Alam M, Schwabe K, Krauss JK. The pedunculopontine nucleus area: Critical evaluation of interspecies differences relevant for its use as a target for deep brain stimulation. *Brain*. 2011;134:11–23.
38. Josset N, Roussel M, Lemieux M, Lafrance-Zoubga D, Rastqar A, Bretzner F. Distinct contributions of mesencephalic locomotor region nuclei to locomotor control in the freely behaving mouse. *Curr Biol*. 2018;28:884–901.e3.
39. Capelli P, Pivetta C, Esposito MS, Arber S. Locomotor speed control circuits in the caudal brainstem. *Nature*. 2017;551:373–377.
40. Caggiano V, Leiras R, Goñi-Erro H, *et al*. Midbrain circuits that set locomotor speed and gait selection. *Nature*. 2018;553:455–460.
41. Opris I, Dai X, Johnson DMG, *et al*. Activation of brainstem neurons during mesencephalic locomotor region-evoked locomotion in the cat. *Front Syst Neurosci*. 2019;13:69.
42. Hofer AS, Schwab ME. Enhancing rehabilitation and functional recovery after brain and spinal cord trauma with electrical neuromodulation. *Curr Opin Neurol*. 2019;32:828–835.
43. Stieglitz LH, Hofer A-S, Bolliger M, *et al*. Deep brain stimulation for locomotion in incomplete human spinal cord injury (DBS-SCI): Protocol of a prospective one-armed multi-centre study. *BMJ Open*. 2021;11:e047670.
44. du Sert NP, Hurst V, Ahluwalia A, *et al*. The arrive guidelines 2.0: Updated guidelines for reporting animal research. *PLoS Biol*. 2020;18:e100115.
45. Watson C, Paxinos G, Kayalioglu G. *The spinal cord: A Christopher and Dana Reeve Foundation text and atlas*: Elsevier, Academic Press; 2009.
46. Keirstead HS, Fedulov V, Cloutier F, Steward O, Duel BP. A noninvasive ultrasonographic method to evaluate bladder function recovery in spinal cord injured rats. *Exp Neurol*. 2005;194: 120–127.
47. Hsieh TH, Tsai JY, Wu YN, Hwang IS, Chen TI, Chen JJJ. Time course quantification of spastic hypertonia following spinal hemisection in rats. *Neuroscience*. 2010;167:185–198.
48. Zörner B, Filli L, Starkey ML, *et al*. Profiling locomotor recovery: Comprehensive quantification of impairments after CNS damage in rodents. *Nat Methods*. 2010;7:701–708.

49. Schindelin J, Arganda-Carreras I, Frise E, *et al*. Fiji: An open-source platform for biological-image analysis. *Nat Methods*. 2012;9:676–682.
50. Basso DM, Beattie MS, Bresnahan JC. A sensitive and reliable locomotor rating scale for open field testing in rats. *J Neurotrauma*. 1995;12:1–21.
51. Ward PJ, Hubscher CH. Persistent polyuria in a rat spinal contusion model. *J Neurotrauma*. 2012;29:2490–2498.
52. Patel A, Li Z, Canete P, *et al*. AxonTracer: A novel ImageJ plugin for automated quantification of axon regeneration in spinal cord tissue. *BMC Neurosci*. 2018;19:8.
53. Paxinos G, Watson C. *The rat brain in stereotaxic coordinates: Compact*. 6th ed. Elsevier, Academic Press; 2009.
54. Koopmans GC, Deumens R, Honig WMM, Hamers FPT, Steinbusch HWM, Joosten EAJ. The assessment of locomotor function in spinal cord injured rats: The importance of objective analysis of coordination. *J Neurotrauma*. 2005;22:214–225.
55. Scheff SW, Saucier DA, Cain ME. A statistical method for analyzing rating scale data: The BBB locomotor score. *J Neurotrauma*. 2002;19:1251–1260.
56. Talpalar AE, Bouvier J, Borgius L, Fortin G, Pierani A, Kiehn O. Dual-mode operation of neuronal networks involved in left–right alternation. *Nature*. 2013;500:85–88.
57. Ruder L, Takeoka A, Arber S. Long-distance descending spinal neurons ensure quadrupedal locomotor stability. *Neuron*. 2016;92:1063–1078.
58. Mitchell EJ, McCallum S, Dewar D, Maxwell DJ. Corticospinal and reticulospinal contacts on cervical commissural and long descending propriospinal neurons in the adult rat spinal cord; Evidence for powerful reticulospinal connections. *PLoS One*. 2016;11:e0155664.
59. Matsuyama K, Nakajima K, Mori F, Aoki M, Mori S. Lumbar commissural interneurons with reticulospinal inputs in the cat: Morphology and discharge patterns during fictive locomotion. *J Comp Neurol*. 2004;474:546–561.
60. Kim LH, Sharma S, Sharples SA, Mayr KA, Kwok CHT, Whelan PJ. Integration of descending command systems for the generation of context-specific locomotor behaviors. *Front Neurosci*. 2017;11:581.
61. Roseberry TK, Lee AM, Lalive AL, Wilbrecht L, Bonci A, Kreitzer AC. Cell-type-specific control of brainstem locomotor circuits by basal ganglia. *Cell*. 2016;164:526–537.
62. Edwards SB, de Olmos JS. Autoradiographic studies of the projections of the midbrain reticular formation: Ascending projections of nucleus cuneiformis. *J Comp Neurol*. 1976;165:417–431.
63. Malmierca MS, Young ED. Inferior colliculus microcircuits. *Front Neural Circuits*. 2014;8:113.
64. Basso MA, May PJ. Circuits for action and cognition: A view from the superior colliculus. *Annu Rev Vis Sci*. 2017;3:197–226.
65. Mitchell AS, Czajkowski R, Zhang N, Jeffery K, Nelson AJD. Retrosplenial cortex and its role in spatial cognition. *Brain Neurosci Adv*. 2018;2:239821281875709.
66. Sébille SB, Belaid H, Philippe AC, *et al*. Anatomical evidence for functional diversity in the mesencephalic locomotor region of primates. *Neuroimage*. 2017;147:66–78.
67. Ditunno JF, Little JW, Tessler A, Burns AS. Spinal shock revisited: A four-phase model. *Spinal Cord*. 2004;42:383–395.
68. Ballermann M, Fouad K. Spontaneous locomotor recovery in spinal cord injured rats is accompanied by anatomical plasticity of reticulospinal fibers. *Eur J Neurosci*. 2006;23:1988–1996.
69. Filli L, Engmann AK, Zorner B, *et al*. Bridging the gap: A reticulopropriospinal detour bypassing an incomplete spinal cord injury. *J Neurosci*. 2014;34:13399–13410.
70. Schucht P, Raineteau O, Schwab ME, Fouad K. Anatomical correlates of locomotor recovery following dorsal and ventral lesions of the rat spinal cord. *Exp Neurol*. 2002;176:143–153.
71. Nathan PW, Smith M, Deacon P. Vestibulospinal, reticulospinal and descending propriospinal nerve fibres in man. *Brain*. 1996;119(Pt 6):1809–1833.
72. Dimitrijević MR. Residual motor functions in spinal cord injury. *Adv Neurol*. 1988;47:138–155.
73. Dimitrijevic MR, Faganel J, Lehmkuhl D, Sherwood A. Motor control in man after partial or complete spinal cord injury. *Adv Neurol*. 1983;39:915–926.
74. Dimitrijevic MR. Neurophysiology in spinal cord injury. *Paraplegia*. 1987;25:205–208.
75. Baker SN, Perez MA. Reticulospinal contributions to gross hand function after human spinal cord injury. *J Neurosci*. 2017;37:9778–9784.
76. Sangari S, Perez MA. Distinct corticospinal and reticulospinal contributions to voluntary control of elbow flexor and extensor muscles in humans with tetraplegia. *J Neurosci*. 2020;40:8831–8841.
77. Pfyffer D, Vallotton K, Curt A, Freund P. Predictive value of midsagittal tissue bridges on functional recovery after spinal cord injury. *Neurorehabil Neural Repair*. 2021;35:33–43.
78. Smith AC, Angeli CA, Ugiliweneza B, *et al*. Spinal cord imaging markers and recovery of standing with epidural stimulation in individuals with clinically motor complete spinal cord injury. *Exp Brain Res*. 2022;240:279–288.
79. Vallotton K, Huber E, Sutter R, Curt A, Hupp M, Freund P. Width and neurophysiologic properties of tissue bridges predict recovery after cervical injury. *Neurology*. 2019;92:e2793–e2802.
80. Rejc E, Smith AC, Weber KA, *et al*. Spinal cord imaging markers and recovery of volitional leg movement with spinal cord epidural stimulation in individuals with clinically motor complete spinal cord injury. *Front Syst Neurosci*. 2020;14:559313.
81. Angeli CA, Boakye M, Morton RA, *et al*. Recovery of over-ground walking after chronic motor complete spinal cord injury. *N Engl J Med*. 2018;379:1244–1250.
82. Karamian B, Siegel N, Nourie B, *et al*. The role of electrical stimulation for rehabilitation and regeneration after spinal cord injury. *J Orthop Traumatol*. 2022;23:2.
83. Seáñez I, Capogrosso M. Motor improvements enabled by spinal cord stimulation combined with physical training after spinal cord injury: Review of experimental evidence in animals and humans. *Bioelectron Med*. 2021;7:16.
84. Courtine G, Sofroniew MV. Spinal cord repair: Advances in biology and technology. *Nat Med*. 2019;25:898–908.
85. Loy K, Bareyre FM. Rehabilitation following spinal cord injury: How animal models can help our understanding of exercise-induced neuroplasticity. *Neural Regen Res*. 2019;14:405–412.
86. Yang JF, Musselman KE. Training to achieve over ground walking after spinal cord injury: A review of who, what, when, and how. *J Spinal Cord Med*. 2012;35:293–304.
87. Morrison SA, Lorenz D, Eskay CP, Forrest GF, Basso DM. Longitudinal recovery and reduced costs after 120 sessions of locomotor training for motor incomplete spinal cord injury. *Arch Phys Med Rehabil*. 2018;99:555–562.
88. Kakulas BA. Neuropathology: The foundation for new treatments in spinal cord injury. *Spinal Cord*. 2004;42:549–563.
89. Lorenz DJ, Datta S, Harkema SJ. Longitudinal patterns of functional recovery in patients with incomplete spinal cord injury receiving activity-based rehabilitation. *Arch Phys Med Rehabil*. 2012;93:1541–1552.
90. Marques MR, Nicola FC, Sanches EF, *et al*. Locomotor training promotes time-dependent functional recovery after experimental spinal cord contusion. *Neuroscience*. 2018;392:258–269.

91. Bonizzato M, James ND, Pidpruzhnykova G, *et al*. Multi-pronged neuromodulation intervention engages the residual motor circuitry to facilitate walking in a rat model of spinal cord injury. *Nat Commun*. 2021;12:1925.
92. Noga BR, Guest JD. Combined neuromodulatory approaches in the central nervous system for treatment of spinal cord injury. *Curr Opin Neurol*. 2021;34:804–811.
93. Groen J, Pannek J, Castro Diaz D, *et al*. Summary of European Association of Urology (EAU) guidelines on neuro-urology. *Eur Urol*. 2016;69:324–333.
94. Valentino RJ, Page ME, Luppi PH, Zhu Y, Van Bockstaele E, Aston-Jones G. Evidence for widespread afferents to Barrington's nucleus, a brainstem region rich in corticotropin-releasing hormone neurons. *Neuroscience*. 1994;62:125–143.
95. Blanco L, Yuste JE, Carrillo-de Sauvage MA, *et al*. Critical evaluation of the anatomical location of the Barrington nucleus: Relevance for deep brain stimulation surgery of pedunculopontine tegmental nucleus. *Neuroscience*. 2013;247:351–363.
96. Verstegen AMJ, Vanderhorst V, Gray PA, Zeidel ML, Geerling JC. Barrington's nucleus: Neuroanatomic landscape of the mouse "pontine micturition center". *J Comp Neurol*. 2017;525:2287–2309.
97. Hubscher CH, Herrity AN, Williams CS, *et al*. Improvements in bladder, bowel and sexual outcomes following task-specific locomotor training in human spinal cord injury. *PLoS One*. 2018;13:e0190998.
98. Martens FMJ, Sievert KD. Neurostimulation in neurogenic patients. *Curr Opin Urol*. 2020;30:507–512.
99. Sartori AM, Salemi S, Hofer A-S, *et al*. Early transcutaneous tibial nerve stimulation acutely improves lower urinary tract function in spinal cord injured rats. *Neurotrauma Rep*. 2022;3:15–26.
100. Peters KM, Carrico DJ, Perez-Marrero RA, *et al*. Randomized trial of percutaneous tibial nerve stimulation *versus* sham efficacy in the treatment of overactive bladder syndrome: Results from the SUmiT trial. *J Urol*. 2010;183:693.
101. Finazzi-Agr E, Petta F, Sciobica F, Pasqualetti P, Musco S, Bove P. Percutaneous tibial nerve stimulation effects on detrusor overactivity incontinence are not due to a placebo effect: A randomized, double-blind, placebo controlled trial. *J Urol*. 2010;184:2001–2006.
102. Herrity AN, Aslan SC, Ugiliweneza B, Mohamed AZ, Hubscher CH, Harkema SJ. Improvements in bladder function following activity-based recovery training with epidural stimulation after chronic spinal cord injury. *Front Syst Neurosci*. 2021;14:614691.
103. Darrow D, Balser D, Netoff TI, *et al*. Epidural spinal cord stimulation facilitates immediate restoration of dormant motor and autonomic supraspinal pathways after chronic neurologically complete spinal cord injury. *J Neurotrauma*. 2019;36:2325–2336.
104. Walter M, Lee AHX, Kavanagh A, Phillips AA, Krassioukov AV. Epidural spinal cord stimulation acutely modulates lower urinary tract and bowel function following spinal cord injury: A case report. *Front Physiol*. 2018;9:1816.